Process Safety and Environmental Protection 184 (2024) 747–765

Contents lists available at ScienceDirect

Process Safety and Environmental Protection

journal homepage: www.journals.elsevier.com/process-safety-and-environmental-protection

Predicting the effects of direct-injected fuels co-powered by high-CO_2 biogas on RCCI engine emissions using kinetic mechanisms and multi-objective optimization

Ibrahim B. Dalha [a,*], Kemal Koca [b], Mior A. Said [c], Aminu D. Rafindadi [d]

[a] Department of Agricultural and Bio-resources Engineering, Faculty of Engineering, Ahmadu Bello University, Samaru, Zaria 1044, Nigeria
[b] Department of Mechanical Engineering, Faculty of Engineering, Abdullah Gül University, Kayseri 38080, Türkiye
[c] Centre for Automotive Research and Electric Mobility (CAREM), Universiti Teknologi PETRONAS, Perak 32610, Malaysia
[d] Department of Civil Engineering, Faculty of Engineering, Bayero University, Kano 3011, Nigeria

ARTICLE INFO

Keywords:
RCCI
High-CO_2 content
Biogas
Emission trade-off
Kinetic mechanisms
Multi-objective optimization

ABSTRACT

High inert gas content in biogas resulted in poor burning and emissions attributes, though scarcely investigated in reactivity controlled compression ignition (RCCI). Established kinetic mechanisms were combined with multi-objective optimization to investigate, predict, and analyze emissions occurrence and trade-offs for reduced environmental impacts. The work examined the impact of direct-injected high reactivity fuels (HRF) and port-injected Biogas at various inert gas (carbon dioxide, CO_2) rates (25 – 45% vol), biogas fractions (40 – 70%), speeds (1600 – 2000 rpm), and loads (4.5 – 6.5 bar IMEP) on emissions of RCCI engine, experimentally. The findings revealed that while engine speeds greatly decreased CO (carbon monoxide) and NOx (nitrate oxide) emissions with rising unburned hydrocarbon (UHC) regardless of HRF employed, higher engine load significantly reduced UHC emissions. Diesel-biogas reduces NOx emissions and performs better in reducing CO and UHC emissions at lower speeds than B5-biogas, except in low-level loads. Although increasing CO_2 impact led to a reduction in UHC and CO emissions, the biogas proportion was the most significant variable. The main factor influencing increased NOx emissions was engine load, which is inversely correlated with reduced NOx and increased particulate emissions owing to high CO_2 content and biogas proportion. The premixed mode's optimisation outcome confirms the trade-off reduction at 5.5 bar IMEP, 35.586% CO_2, and 50% fraction. As a result, running the RCCI engine with direct-injected diesel co-powered in equal proportion with high-CO_2 biogas cuts the emissions trade-off dramatically, limiting the environmental repercussions of the emissions.

1. Introduction

Engine emissions are an incredible source of pollution that is environmentally harmful (El-Adawy, 2023; Li et al., 2023; Polat, 2022) Epidemiological figures reveal that, in particular, prolonged exposure to emissions detrimentally causes injuries to human health (Merk et al., 2020). Carbon monoxides (CO) emissions affect human health by weakening the blood's oxygen gas (O_2) carrying ability, thereby displacing it from the haemoglobin in the lung (Russell et al., 2002). Incomplete combustion also contributes a substantial fraction of toxic air contaminants, such as aldehydes and benzene, that poses some carcinogenic risk for which CO emission control strategies may reduce (Russell et al., 2002). The leading cause of climate change is the rising quantity of carbon dioxide (CO_2) and unburned hydrocarbon (UHC) such as methane (CH_4), in the atmosphere as greenhouse gases (GHG) (Meng et al., 2023; Musa et al., 2020). The prime emissions that generate photochemical smog are nitrogen oxides (NOx) and non-methane UHC. In addition to human health effects, NOx also produces acid rain and nitrate particles that degrade stratospheric ozone (Sher, 1998). Exhaust particulate matter (PM) emission from engines leads to swelling, oxidative stress, and cells' death (Borlaza et al., 2018; Merk et al., 2020). PM emission also causes purported cancer growth processes (Popadić et al., 2018) and promotes pulmonary diseases (Hopke and Hill, 2021). Exposure to pollution from the burning of biomaterial-based (Barabad et al., 2018) and conventional fuels (Edwards et al., 2021) has been linked to asthma and tuberculosis. The rising amount of pollution has prompted an in-depth quest for an alternative fuel derived from renewable sources (Hosseini and Wahid, 2013). Utilizing renewable low reactivity fuel (LRF) in conjunction with conventional fuels has

* Corresponding author.
E-mail addresses: ibdalha@abu.edu.ng, ibrahim_16005836@utp.edu.my (I.B. Dalha).

https://doi.org/10.1016/j.psep.2024.02.026
Received 27 December 2023; Received in revised form 28 January 2024; Accepted 11 February 2024
Available online 15 February 2024

Nomenclature

2D	two dimensional
2FI	two factor interaction
3D	three dimensional
ABU	Ahmadu Bello University
AGU	Abdullah Gul Uninversity
ANOVA	analysis of variance
AP	adequate precision
B5	5% Biodiesel
BBD	Box Behnken design
BTDC	before top dead centre
CA	crank angle
CAREM	centre for automotive research and electric mobility
CDC	conventional diesel combustion
CH_3	methyl radical
CH_4	methane gas
CO	carbon monoxide
CO_2	carbon dioxide
CR	compression ratio
GHG	greenhouse gas
H	hydrogen radical
H_2O_2	hydrogen peroxide
HRF	high reactivity fuel
IC	internal combustion
IMEP	indicated mean effective pressure
LRF	low reactivity fuel
N	nitrogen
NG	natural gas
NOx	nitrogen oxides
O	oxygen
O_2	oxygen gas
OH	hydroxyl radical
PM	particulate matter
PRC	PETRONAS research centre
R^2	correlation coefficient
RCCI	reactivity controlled compression ignition
RSM	response surface methodology
SD	standard deviation
UHC	unburned hydrocarbon
UTP	Universiti Teknologi PETRONAS

demonstrated enormous promise to mitigate some of the effects of present-day pollution (W. Li et al., 2016), including the development of more sophisticated techniques like RCCI (reactivity-controlled compression ignition) combustion (Hopke and Hill, 2021).

Mixing different fuels in the cylinder to influence and boost the burning rate through layers formation is referred to as RCCI combustion (Ibrahim B. Dalha et al., 2020; J. Li et al., 2017). High reactivity fuel (HRF) auto-ignition triggers combustion, while increasing thermal gradients promotes the burning process of port-induced fuel (Benajes et al., 2014). The technique became a fascinating approach but remained prone to an in-depth review of its precision (Salahi et al., 2017). The mode allows high thermal efficiency to be realized while cutting NOx and PM emissions. Nevertheless, attempting to reduce those emissions causes unsustainably rised UHC and CO discharges (Firmansyah et al., 2017). However, Agarwal et al. [5] indicated that studies should provide more techniques for reducing UHC and CO discharge in their report. The use of fuel gas is among the steps, although Li et al. (Y. Y. Li et al., 2017) stated that high UHC and CO emissions are also emitted by natural gas (NG) and diesel combustion. While different analyses were performed under RCCI combustion using liquid biofuels and NG, in addition to several studies to understand the efficacy of biogas under other multi-fuel combustion techniques, little efforts were devoted to biogas application in RCCI (Barik and Murugan, 2016; Shan et al., 2016). This fact inspired the authors to embrace the RCCI combustion mode for sufficient utilization of biogas (Gund et al., 2017). CH_4, CO_2, and a limited proportion of nitrogen, although a substantial portion of unacceptable residues, like sulfur compounds, among others, constitute primarily biogas derived through anaerobic processing of biological materials as a fuel for automobiles (Bora and Saha, 2016). It is a vital green energy source with numerous potential uses and can substitute NG in internal combustion (IC) engines and prevent its ecological risk (Duic et al., 2016). Table 1 reveals that biomass-based biogas comprises 35 – 80% CH_4, 20 – 55% CO_2, some nitrogen elements, and other unacceptable substances. Impurities in biogas are mostly a result of their origin and may be damaging to engines (Ullah et al., 2017) and the environment. Different dual-fuel processes came up to minimize the emissions mechanically but induce some risk that sabotages the efforts towards achieving the standard limits (Soni and Gupta, 2016). The information necessary to evaluate the flow of engine operations and the control strategies to concurrently reduce harmful emissions for biogas remains incomplete. The effect of 0.28% CO_2 gaseous fuel on RCCI engine combustion and emissions was studied by Kakaee et al. (Kakaee et al., 2015). Wang et al. (Wang et al., 2016) examined the probability of utilizing biogas of poor quality with minor or no CO_2 content. These, among other studies, inspired the writers to explore the viability of elevated-CO_2 fraction biogas. As shown in the literature (Ebrahimi and Jazayeri, 2019; Mahmoodi et al., 2020; Qian et al., 2017; Shan et al., 2016; Wang et al., 2016), majority of prior works on differents artificial biogas formulations utilized in RCCI combustion do not symbolize actual biogas.

Table 1
Biomass-based biogas compositions from various sources.

S/N	Source	Major compositions		Ref.
		CH_4	**CO_2**	
1	Caw dung	45 – 80%	20 – 55%	(Gupta and Mittal, 2019)
2	Animal manure	50 – 70%	30 – 50%	(Nwokolo et al., 2020)
3	Mesophilic fermentation	60%	40%	(Xu et al., 2015)
4	Landfill gas	50 – 55%	37 – 45%	(Lamb, 2020)
5	Sewage	55 – 65%	35 – 45%	(Rasi, 2009)
	Organic waste	60 – 70%	30 – 40%	
	Landfill gas	45 – 55%	30 – 40%	
6	Landfill gas	55.63%	37.14%	(Eklund et al., 1998)
7	Dairy waste	50 – 70%	20 – 45%	(Li et al., 2019)
	Food waste	52 – 57%	35 – 46%	
	Landfill gas	35 – 50%	18 – 25%	
8	Mahua seedcake	68 – 72%	28 – 31%	(Deshpande et al., 2012)
9	Algae	60%	30%	(Montingelli et al., 2015)
10	Seaweed algae	50 – 70%	30 – 45%	(Milledge et al., 2019)
	Average	51.31 – 59.5%	30.01 – 38.92	

Moreover, the advantages of using biodiesel, as HRF that enhances fuel stratification and controls the combustion process, are the greatest priority in RCCI combustion. Different proportions of biodiesel derived from renewable sources increase some pollutants, such as NOx, but result in lower emissions of CO, UHC, and PM (Meng et al., 2023; Tizvir et al., 2023). Biodiesel blend below 21% has fewer harmful impacts on

the combustion mechanisms requiring slight or no changes (Saxena et al., 2013). As noted from previous reports, limited attempts were made to explore, in RCCI, the advantages of biodiesel mixtures. Benajes et al. (Benajes et al., 2015) examined the performance of 7% biodiesel and various LRFs experimentally. In their study, Isik and Hüseyin (Isik, Hüseyin, 2016) investigated 10, 20, and 50% biodiesel and ethanol attributes in RCCI. Kalsi and Subramanian (J. Li et al., 2016) reported the characteristics of higher fractions covering 60 – 80% biodiesel in reactivity with hydrogen in compressed NG. Thus, the performance of 5% biodiesel and biogas in RCCI is still evolving. The authors' previous study, (Ibrahim B Dalha et al., 2020), observed elevated emissions at 2000 rpm, which motivated investigation at lower engine speed for proper inference. The article presents an optimization and experimental analysis in a premixed RCCI mode on the effect of direct-injected fuels at different operational conditions and biogas containing elevated CO_2 at various rate and fractions. Using kinetic mechanisms, the effects of these parameters on emission occurrences were also predicted and analysed. To the best of the author's knowledge, the optimal influence of high-CO_2 biogas on combustion and emissions is first analyzed and reported by this research. This paper also pioneered the use of established kinetic mechanisms along with multi-objective optimization to analyze emissions occurrence and trade-offs. In addition to the conventional approach, the work has demonstrated that the kinetics of fuel combustion analysis increases experimental understanding of emissions occurrences. The work provides more insight into emissions and their trade-off as serious setbacks in RCCI combustion that could be reconciled through port injection of biogas containing high CO_2. Therefore, our results will add to the rapidly increasing field of RCCI combustion and emission reduction techniques aiming to minimize some of the impacts of present-day pollutants such as climate change and the risk of exposure to detrimental diseases.

2. Methodology

2.1. Set-up and Test Equipment

To achieve biogas injection for dual-fuel, a Yanmar diesel engine described in Table 2 was modified as depicted in Fig. 1. The engine was modified by incorporating anjector holder that carries the biogas injection valve connected to the biogas cylinders through a delivery hose. More details of the engine modifications and the experiment's measurements of engine load, speed, crank angle, mass flow rate, and volume are reported in the research papers (Dalha et al., 2020; Dalha et al., 2021, 2022; Said et al., 2021). The study analyzed the impact of direct-injected diesel and B5 as HRFs and premixed biogas with high-CO_2 on RCCI engine emissions at various loads and speeds.

2.2. Test procedure and fuel

The experiment was performed to analyze the engine attributes in premixed mode at different speeds (1600, 1800, and 2000 rpm) and low load (4.5, 5, 5.5, 6, and 6.5 bar IMEP) conditions. According to (Bortel et al., 2017; Gharehghani et al., 2015), the HRF supplied at different loads to keep the fractions of 40%, 50%, 60%, and 70% was used to compute the mass of biogas. Biogas fractions of 40 – 70% were port-injected for each of the 25, 35, and 45% CO_2 proportions at the loads mentioned above.The experimental process flow is depicted by the chart in Fig. 2. To improve in-cylinder blending (Kavuri et al., 2016; Wang et al., 2016), an advanced 21° CA BTDC timing of injection was adopted. The biogas was delivered at 110 mm downstream of the valve position. The biogas was induced at various flow rates to balance the HRF fractions while maintaining an unchanged pressure of 2 bar. Table 3 depicts how the experimental repeatability of the work was determined using the procedure given by (Barik and Murugan, 2016).

Table 2
Detail of the test machine utilized.

Synopsis	Specifications
Engine Model	L100V
Engine Type	Air-cooled 4-stroke single-cylinder (Yammer Diesel)
Cylinder Bore/Stroke	86/75 mm
Volume (Displacement)	435 cm^3
CR (ratio of compression)	20.0 ± 0.3
Timing (Injection)	21° CA BTDC (crank angle before top dead centre)
Injector Type	Bosh
Injection Pulse	Single
Injection Angle	83.38°
Injection Pressure	200 bar
Injector Holes	4
Injector Spray Angle	13.35°
Maximum Rated Output	Power (6.8 kW) and speed (3600 rpm)

2.2.1. Optimization method

The Box Behnken Design (BBD) of response surface methodology (RSM) was used to optimize the biogas in-cylinder mixing variables. The optimization aims at minimizing UHC, CO, NOx, and particulate (PM) emissions of the RCCI in premixed combustion at medium loads as response variables. The independent variables at three levels each are; engine load (5.5, 6, and 6.5 bar IMEP), CO_2 contents (25, 35, and 45%), and biogas fraction (50, 60, and 70%). The optimization conditions involve 12 runs, for low and high levels, with the three center points as additional runs making 15 runs in a randomized manner. The independent variables were optimized, and the models for the responses were developed based on the best fitting relationship. The optimization process flow chart is depicted in Fig. 3.

2.2.2. Fuels used

The study examines the performance of Euro 2 M diesel supplied by the PETRONAS Research Center (PRC) as pilot fuel in RCCI mode. An average from the various sources of biogas resulted in approximately 50 – 60% CH_4 and 30 – 40% CO_2, as shown in Table 1. Thus, three different compositions to simulate pure raw biogas were supplied from Linde Malaysia, a gas firm, for port-injection; Biogas 1 (75% CH_4, 25% CO_2), Biogas 2 (65% CH_4, 35% CO_2), and Biogas 3 (55% CH_4, 45% CO_2). Table 4 displays some of the properties of the fuels used. The properties of the direct-injected fuels were obtained directly from the supplier. Some of the properties of Biogas used also obtained from the supplier while others were calculated as the mixture containing known gaseous CH_4 and CO_2 compounds. The properties of CH_4 and CO_2 gases are well established in the literature.

3. Results and discussion

3.1. Influence of HRFs and operational conditions on the emissions

The effect of fuel reactivity at varying conditions on several emission parameters was investigated.

3.1.1. Effects on CO emission discharged to the environment

According to Fig. 4a, the CO emission rises at mid-5.5 bar IMEP while decreasing as it approaches full capacity for B5-biogas combustion at 1800 and 2000 rpm. Low cylinder temperature at 5.5 bar IMEP, could likely be the reason for high CO emission at this particular load for both fuels. Besides, the CO emission at 1600 rpm demonstrates a steady rise, peaking at 6–6.5 bar IMEP because the CO is released at 1600 rpm while oxidized at higher speed levels. The highest CO emission was found at 1800 rpm for B5-biogas at 4.5–5.5 bar IMEP. Likely because of more hydrogen (H) and methyl (CH_3) radical oxidation under lean condition. The highest emission occurred at mid-load for all the engine speeds, except 1600 rpm, which is because of similar oxidation processes. Compared to 2000 rpm, the emission reduces by 11.11–21.43% at light load using 1600 rpm for B5-biogas. A lowest 0.11% CO discharge at 4.5 bar IMEP for B5-biogas, was found 59.49% higher than the standard

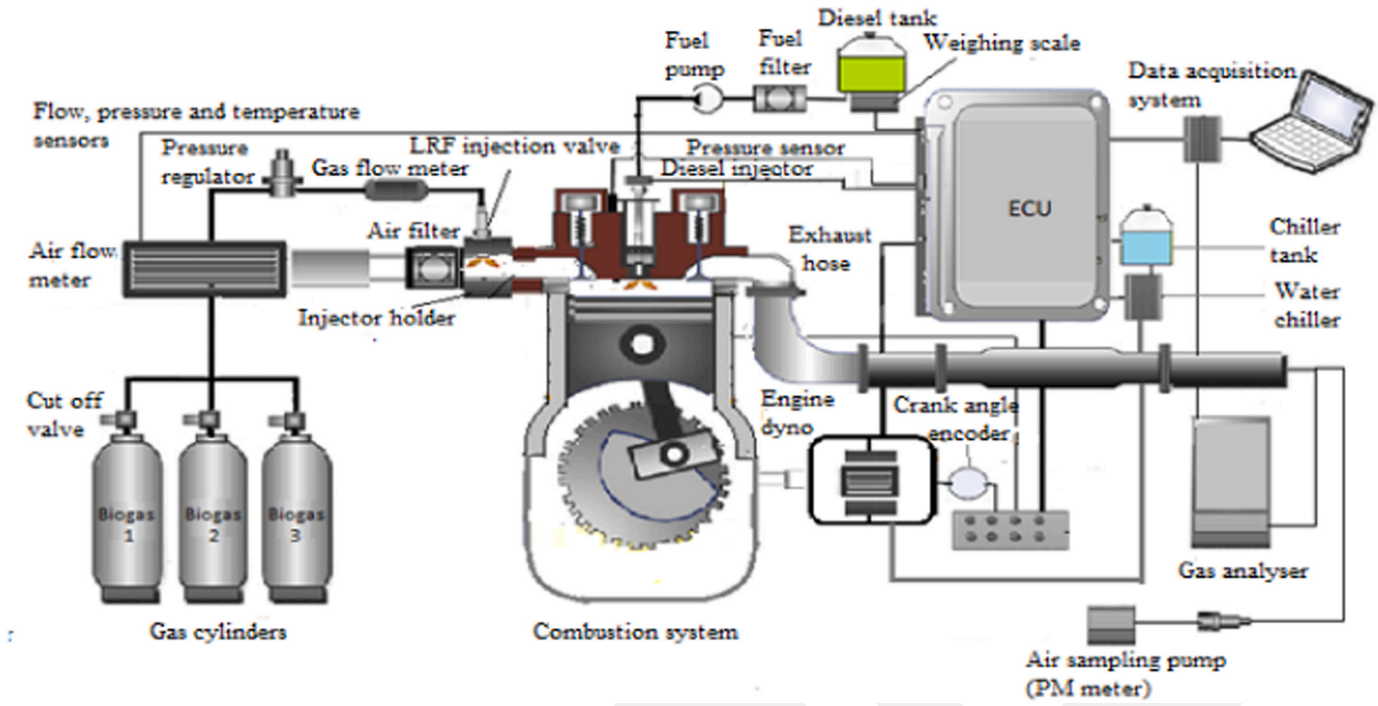

Fig. 1. A description of the experimental test engine (Dalha et al., 2020).

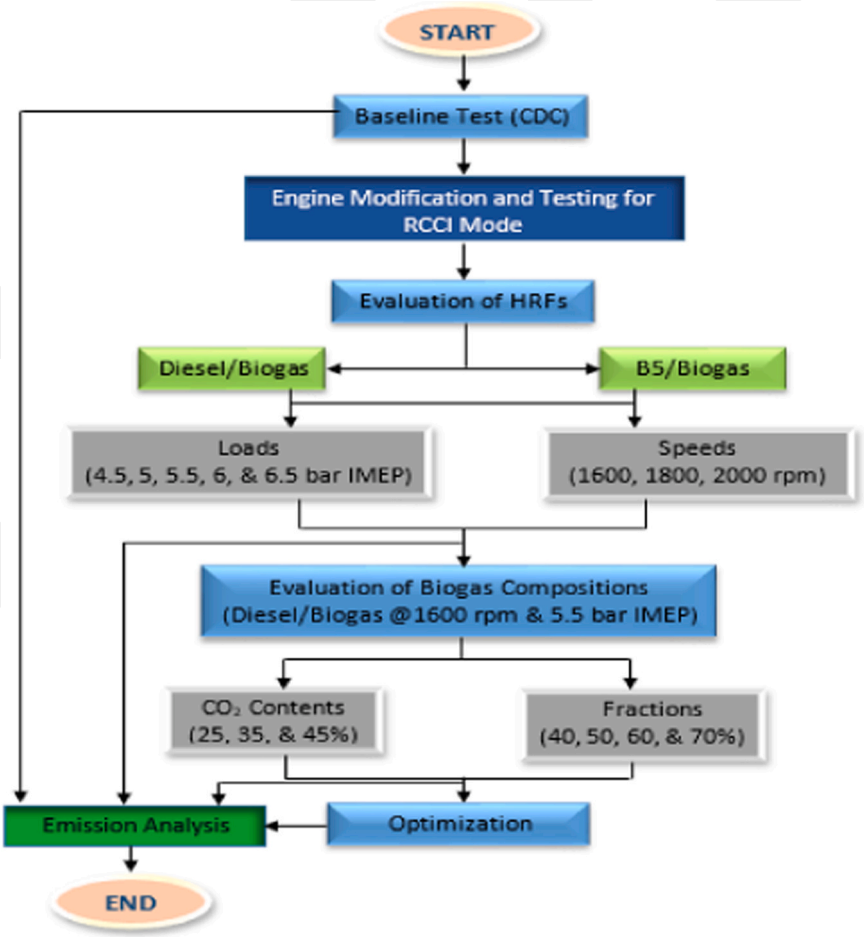

Fig. 2. Experimental process flow chart.

Table 3
Some dependent and independent variables' reliability and uncertainty.

Parameters	Accuracy	Uncertainty
Pressure	0.5% FS	±1.82
Crank angle	1μs	±0.14
Torque	±0.25 Nm	±0.83
Speed	±30 rpm	±0.50
CO_2	0.01%	±1.65
CO	0.01%	±0.06
UHC	1 ppm	±1.10
NOx	1 ppm	±0.86
PM	1 ppm	±2.61
Overall experimental uncertainty		±3.97

EURO VI limit. Compared to B5-biogas, diesel-biogas demonstrated similar characteristics with the increased engine load for all the speed levels, as shown in Fig. 4b. Contrarily, a pattern of escalated CO emission because of rised engine speed happened at 4.5–5.5 bar IMEP with a reverse pattern at 6.5 bar IMEP. Higher temperature with complete combustion could be the reason for less CO emission at 1600 rpm. According to Ithnin et al. (Ithnin et al., 2015), high CO_2 emission demonstrates more combustion efficiency. A lowest 0.12% CO discharge at 4.5 bar IMEP for diesel-biogas, was found 62.87% higher than the standard limit. The observed emission has a reasonable agreement with the literature (Ambarita, 2017; X. Wang et al., 2016). Compared to the conventional diesel combustion (CDC) at 1600 rpm, RCCI combustion lowers the CO emission at low loads, especially for diesel-biogas, as shown in Fig. 4c. The lower CO emission at low load could contribute to higher CO oxidation for the RCCI combustion. At 6.5 bar IMEP, the trend might have changed cousing high CO during RCCI combustion, most likely as a result of the oxidation of radicals of CH_3 and H in a lean environment with a high diluent ratio, which increased the generation of CO at high temperatures (Fischer and Jiang, 2015). More such characteristics occurred at 1800 rpm across the loads but 5 bar IMEP, as illustrated in Fig. 4d. Even at 5 bar IMEP, the trend shows a same amount of CO emission from all combustion modes attributable to the balance in energy supply by the reactivity fuels leading to the same thermodynamic cylinder condition.

3.1.2. *Effects on UHC emission discharged to the environment*

Fig. 5a illustrates that with the raised engine speed for the different loads, the UHC emission for the B5-biogas combustion declined progressively. This pattern is possibly due to increased cylinder temperature across the loads leading to lower UHC emissions while the discharge escalates at low speed because of the trapped fuel. A significant disparity in UHC emissions was also seen in Fig. 5a as the speed rose to 1800 rpm than 2000 rpm. The emissions decreases with the increase of speed to 2000 rpm. This pattern has shown a difference in the heat capacities of the cylinder charge as the speed increases and will most likely be consistent as it rises more. Because there was a more substantial difference between 1600 and 1800 rpm than between 1800 and 2000 rpm. Compared to 2000 rpm, the emission increases averagely by 42.01%

Table 4
Features of the test fuels.

Properties	Biogas 1	Biogas 2	Biogas 3	Diesel	B5 Diesel
Proportion by volume	25% CO_2	35% CO_2	45% CO_2		
Density (kg/m^3)	1.353	1.563	1.772	820 – 832	823.45
Flammability limit (mol%)	6.1 – 22.4	6.9 – 25.4	8.3 – 30.3	0.6 – 7.5	0.75 – 4.6
Molecular weight (g/mol)	23.5132	25.928	28.896	168	174
Specific gravity at 0°C	1.05	1.21	1.37	0.85	0.852
Specific volume (m^3/kg)	0.739	0.640	0.564	1.18–1.22	
Kinematic viscosity (cSt)	12.74	11.34	9.61	1.5 – 5.8	1.5 – 5.8
Lower heating value (MJ/m3)	26.24	23.15	19.35	36.0	45.139
Stoichiometric Air/ Fuel ratio	14.72:1	13.64:1	12.13:1	15.05:1	14.97:1
Oxygen content (% by mass)				0	0.54 – 0.62
Water content (mg/ kg)				22.916	95.067
Cetane number				59.8	56.1
Octane number	>130	>130	>130		

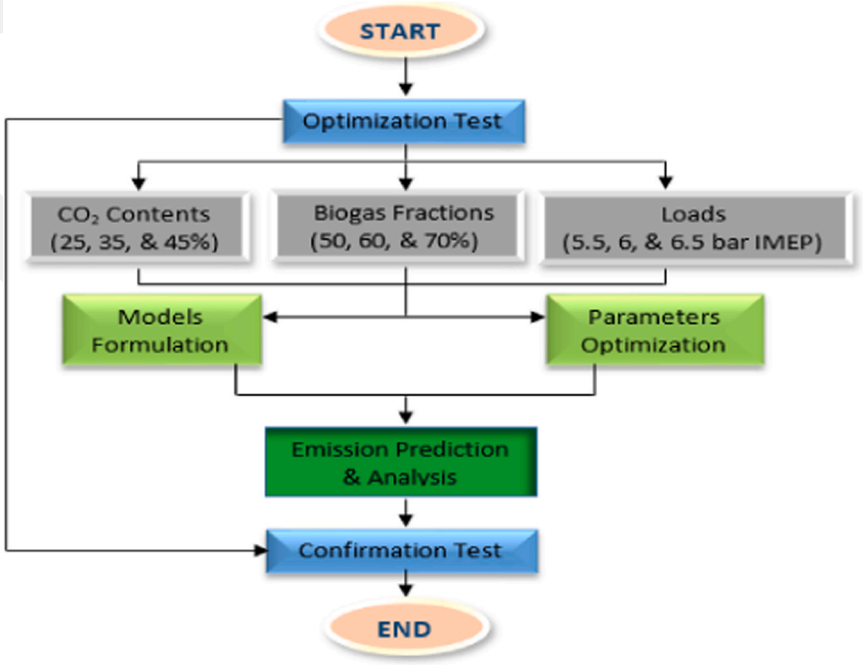

Fig. 3. Optimization process flow.

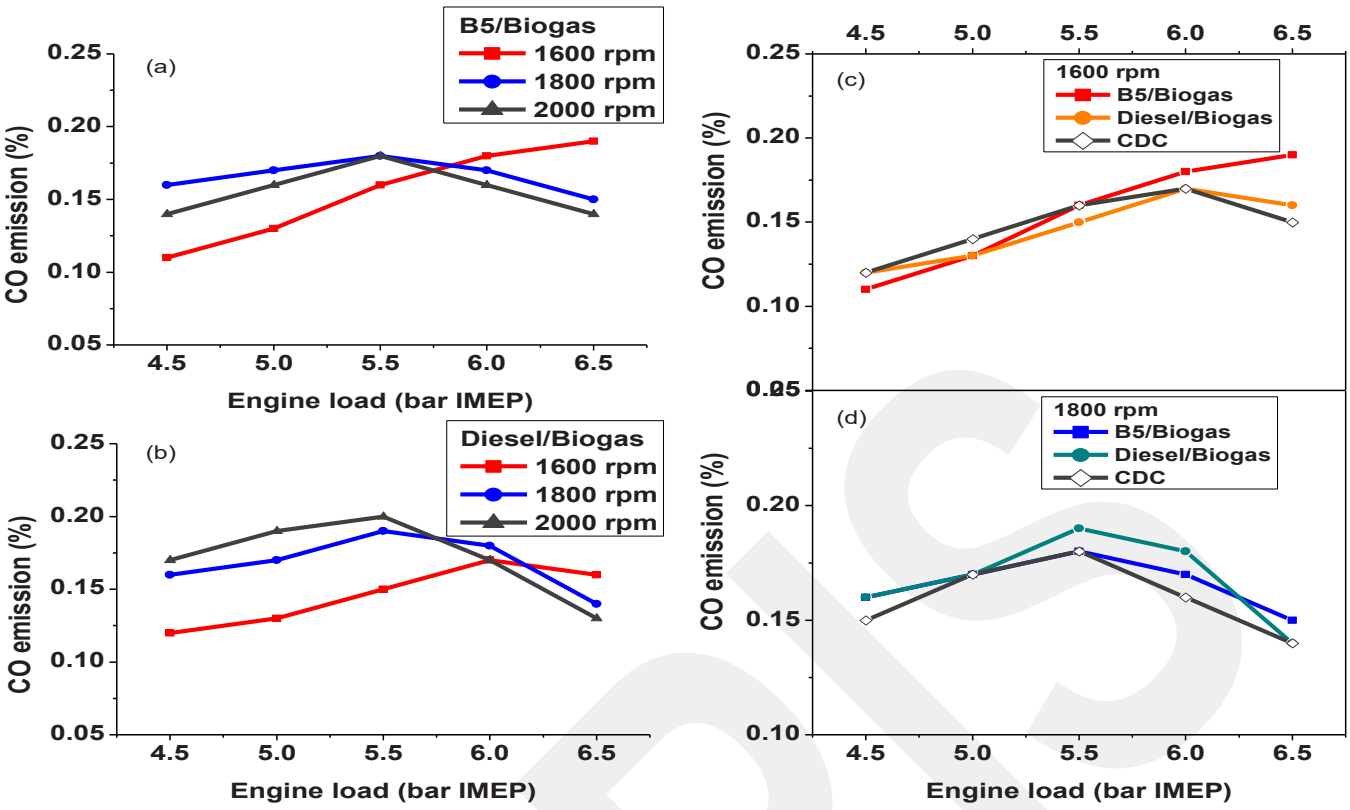

Fig. 4. CO emission for; (a) B5-Biogas, (b) Diesel-Biogas, (c) HRF at 1600 rpm, and (d) HRF at 1800 rpm.

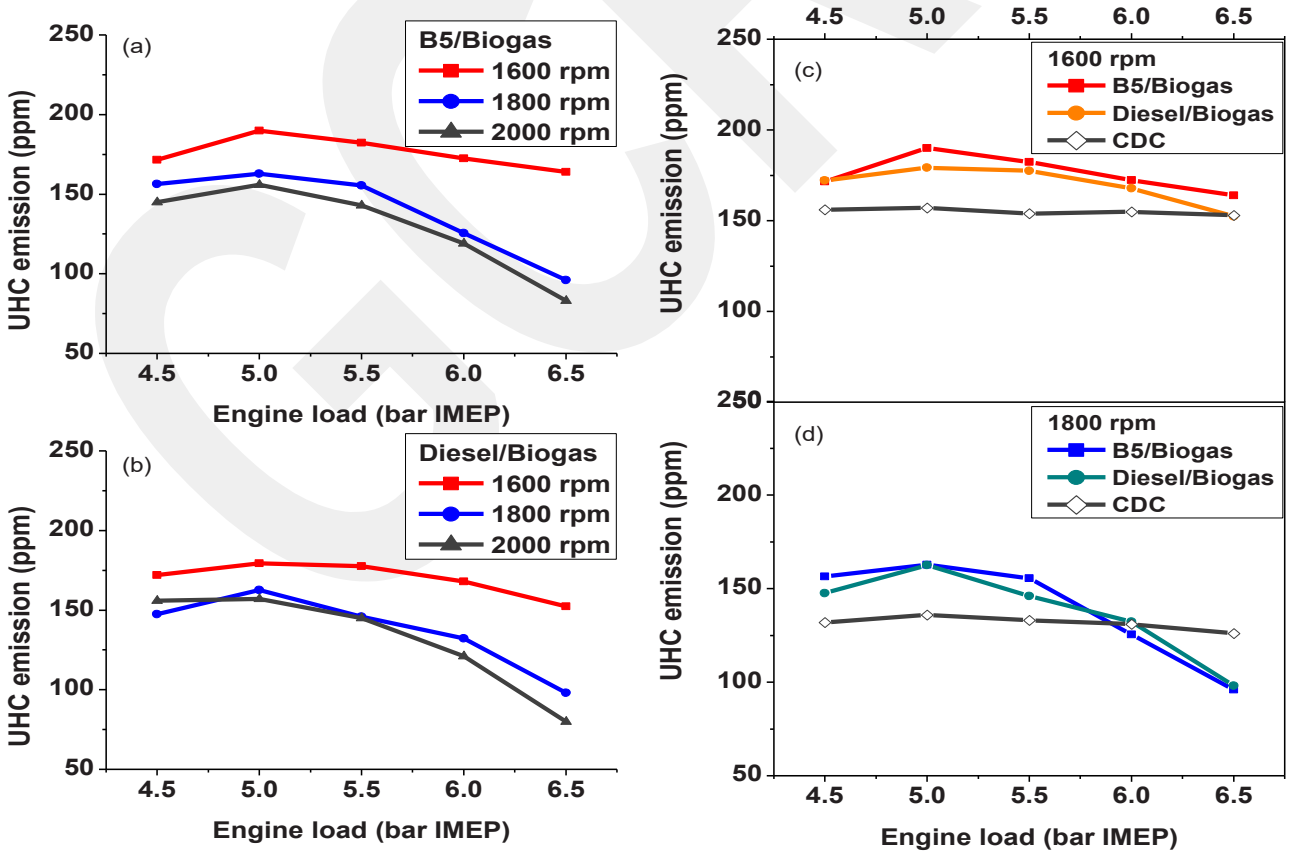

Fig. 5. UHC for; (a) B5-Biogas, (b) Diesel-Biogas, (c) HRF at 1600 rpm, and (d) HRF at 1800 rpm.

across the load at 1600 rpm for B5-biogas. Compared to B5-biogas, diesel-biogas demonstrated similar attributes of decrease with the increased loads but 4.5 bar IMEP. At a 4.5 bar IMEP, a speed of 1800 rpm emitted the lowest UHC, probably due to less fuel trapped in the crevices or high cylinder temperature than 2000 rpm. The emission increases averagely by 35.24% across the loads for diesel-biogas at 1600 rpm. Though the emission increases at 1600 rpm, a minimum of 152.38 ppm was observed at 6.5 bar IMEP, 63.90% lower than the standard limit. Relative to CDC, RCCI combustion showed a considerably higher UHC emission at 1600 rpm for all the loads, as shown in Fig. 5c. The high UHC emission could be due to premixed biogas during RCCI combustion, which might occupy the crevice region along with the air. 1800 rpm, similarly, shows the disadvantage of high UHC emission during RCCI combustion across the loads except full 6.5 bar IMEP illustrated in Fig. 5d. The low UHC emission at full load could be due to a significantly raised temperature during RCCI combustion, unlike CDC. Thus, causing a relatively high UHC emission at full capacity for the CDC, unlike RCCI combustion, as depicted in both Figs. 5c and 5d. The findings are congruent with the existing research (Ambarita, 2017; Wang et al., 2016).

3.1.3. *Effects on NOx emission discharged to the environment*

Owing to the rised temperature in the cylinder for B5-biogas combustion, NOx emissions elevated due to expanded engine speed for the different loads, as shown in Fig. 6a. The NOx emission was relatively similar at 4.5–5.5 bar IMEP, especially at 1600 and 1800 rpm, unlike 2000 rpm with high discharge. The NOx emissions considerably increase when the load increases from 5.5 bar IMEP to 6.5 bar IMEP because of elevated cylinder temperature. However, the margin between 1600 rpm and other speed levels increased with raised engine capacity due to elevated cylinder temperature, causing a high nitrogen (N) – Oxygen (O) bond formation when operated at higher speeds. Compared to 2000 rpm, the emission decreases averagely by 62.87% across the load at 1600 rpm for B5-biogas. Diesel-biogas demonstrated similar characteristics of reduced NOx emission for 1600 and 1800 rpm, as shown in Fig. 6b. Unlike B5-biogas at 2000 rpm, diesel-biogas indicated firmly the same NOx emission at low loads relative to other speed levels. Compared to 2000 rpm, the emission decreases averagely by 43.06% across the load at 1600 rpm for diesel-biogas. The lowest NOx emission of 1 ppm was observed at 4.5 bar IMEP, substantially lower than the standard limit. These results reflect those of (X. Wang et al., 2016).

Relative to CDC at 1600 rpm, RCCI combustion lowered the NOx emission significantly across the loads because of reduced cylinder temperature. According to (Paykani et al., 2016), lower heat transfer losses of RCCI cause lower NOx emission compared to CDC. 1800 rpm indicated similar characteristics of lower NOx emissions, but the significance of the emission reduction is less than1600rpm, as shown in Fig. 6c and Fig. 6d, respectively. For both speeds of 1600 rpm and 1800 rpm, the emission reduction ability is greater at high load levels due to a large temperature rise.

3.2. *Effects of Biogas Intake Compositions on the Emissions Attributes*

Experimentations were conducted using 25% CO_2 at a biogas fraction of 50%, which resulted in high emissions. Although engine speed was an influential factor, CO_2 content and biogas fraction might also have significant influence on engine-out emissions. This section optimize the effects of various CO_2 proportions and biogas fractions for Diesel-biogas to further reduce environmentally harmful emissions for the RCCI engine. RSM in a BBD was used to optimize and analyze the relationship and interactive effects of the input variables (load, CO_2 content, and biogas fraction) to appropriately understand and manage the exhaust emission. Table 5 depicts the design of the test and the outcomes. Befitting quadratic models were developed to predict CO and UHC emissions. Initially, a quadratic equation was also suggested to estimate the NOx emission with a maximum to a minimum input ratio of

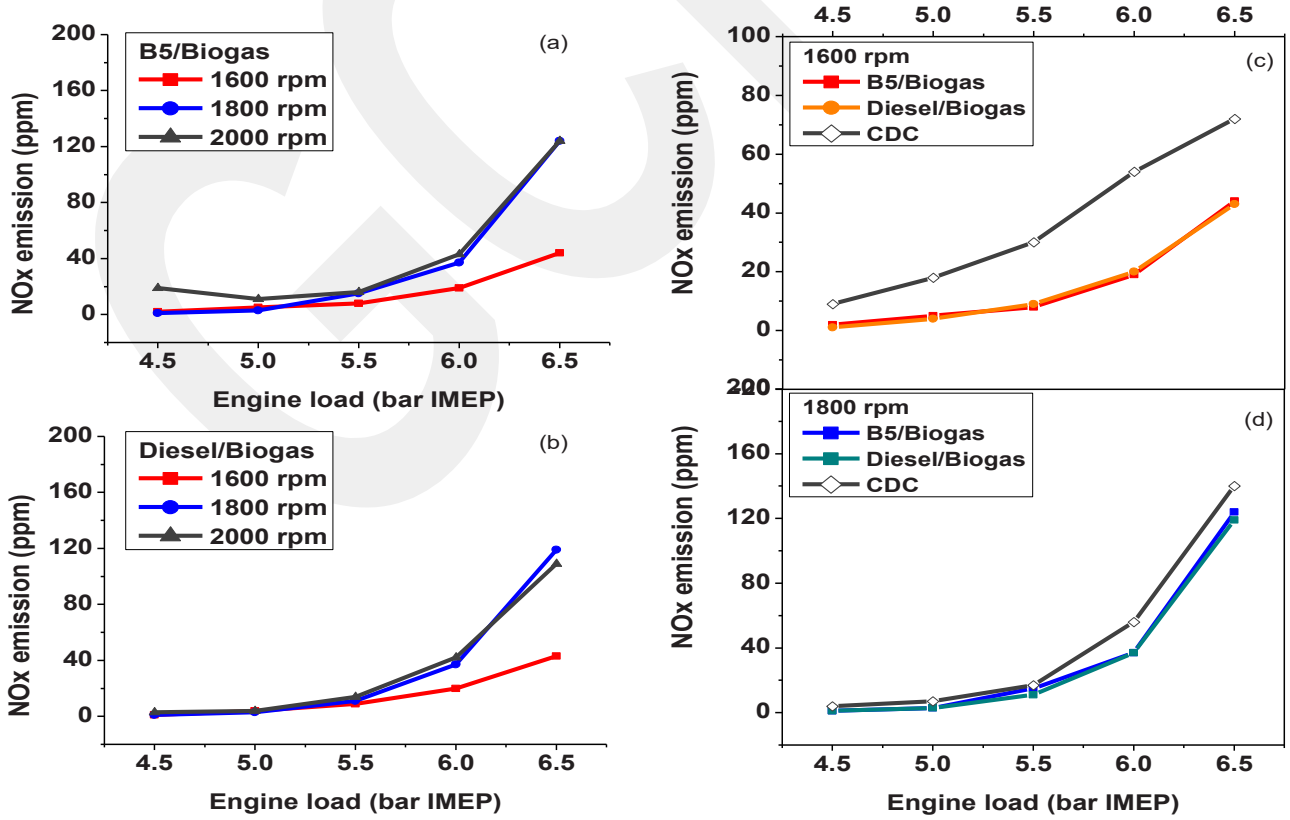

Fig. 6. NOx for; (a) B5-Biogas, (b) Diesel-Biogas, (c) HRF at 1600 rpm, and (d) HRF at 1800 rpm.

Table 5
Experimental design input variables and responses.

Run order	Standard order	Intake parameters			Response set 1			
		Medium Load (bar IMEP)	*CO_2 Contents (%)*	*Biogas fraction (%)*	CO (%)	UHC (ppm)	NOx (ppm)	PM (ppm)
1	11	6	25	70	0.20	326.50	5.34	11.34
2	13	6	35	60	0.17	188.27	14.25	17.00
3	12	6	45	70	0.21	243.08	3.56	23.43
4	2	6.5	25	60	0.17	216.02	32.50	8.31
5	15	6	35	60	0.17	187.48	14.25	17.19
6	9	6	25	50	0.17	170.00	11.88	15.87
7	1	5.5	25	60	0.16	212.95	7.00	6.80
8	5	5.5	35	50	0.13	134.94	7.00	10.58
9	10	6	45	50	0.15	115.98	13.66	22.29
10	8	6.5	35	70	0.17	244.40	22.50	18.89
11	6	6.5	35	50	0.14	120.46	50.00	16.25
12	4	6.5	45	60	0.15	137.26	45.00	20.03
13	14	6	35	60	0.16	189.07	14.84	17.00
14	7	5.5	35	70	0.15	238.96	3.00	20.78
15	3	5.5	45	60	0.13	139.86	5.00	25.70

16.667. Still, a model with a ratio greater than ten (10) requires transformation. However, the initial quadratic model was transformed into a best-fitting square root model based on the analysis of the Box-Cox plot for power transform, which shows an index of 0.5 closed to the recommended 0.32. Contrary to other responses, a two-factor interaction (2FI) model was developed to predict the PM emission. The models were identified and selected among the highest order polynomials based on diagnostic analysis of not aliased parameters.

3.2.1. *Effects biogas intake composition on CO emission attributes*

3.2.1.1. Environmental CO emission interpretation using kinetic mechanism. Experimentally, at 5.5 bar IMEP, Fig. 7a demonstrates that for all diluent CO_2 ratios, CO emission rises as the biogas fraction escalates. Using a 25% diluent rate indicates a relatively the same CO emission at 40 and 50% biogas fraction, then elevates and maintained the same level at 60–70%. In contrast, a gradual increase occurs using 35 and 45% CO_2 ratios, indicating high CO emissions with elevated fraction. The elevated CO emissions due to increased biogas fraction could be an influence of oxidized radicals of H and CH_3 under a lean environment, increasing the CO and NOx formation (Eq. 1 and Eq. 2) (Fischer and Jiang, 2015). It implies that H and CH_3 radical oxidation's impact was less with 25% CO_2 at 5.5 bar IMEP, relatively more complete combustion might happen, reducing the toxic pollutants and risk of affecting human health. Fig. 8

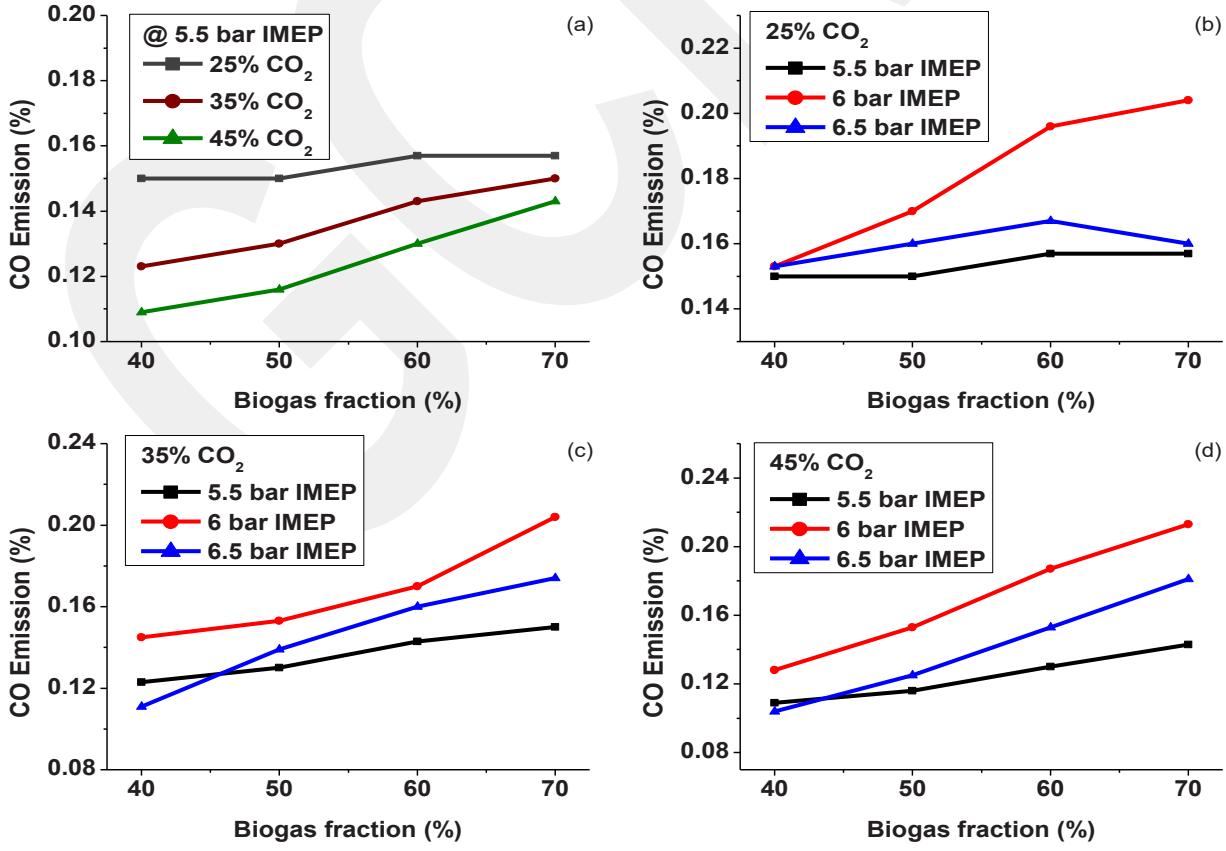

Fig. 7. CO emission at (a) 5.5 bar IMEP, (b) 25% CO_2, (c) 35% CO_2, and (d) 45% CO_2.

$$H + O_2 \leftrightarrow OH + O \quad (1)$$

$$O_2 + CH_3 \rightarrow O + CH_3O \quad (2)$$

$$2CH_3 + M \rightarrow C_2H_6 + M \quad (3)$$

Conversely, for all biogas fractions, the CO emission falls with increasing diluent CO_2 level. Reduced CO emissions in the event of increased CO_2 could be attributed to the recombination of decomposed CH_3 radicals in the elevated temperature phase (Eq. 3) (Fischer and Jiang, 2015). Because 35% CO_2 registered the maximum temperature in Fig. 6a, it appears that fluctuating cylinder temperature might not be the main cause of the CO release. Increasing biogas fractions from 40% to 70% increases CO emissions by 4.46, 18.00, and 23.78% for 25, 35, and 45% CO_2. Also, increasing CO_2 content from 25% to 45% decreases CO emissions by 37.61, 29.31, 20.77, and 9.79% for 40, 50, 60, and 60% fraction, respectively. The lowest emission of 0.109% was registered at a 40% fraction for a 45% CO_2 ratio. The lowest value is still higher than the minimum standard by 59.12%.

Fig. 7b shows that CO emissions patterns are pretty close at various loads over the biogas fractions. A 25% diluent ratio for 5.5 bar IMEP suggests a steady rise in CO emission as the biogas portion advances to 70%. In contrast to the 6 bar IMEP, Fig. 6b shows that a higher proportion of biogas with 25% CO_2 results in a comparatively lower peak cylinder temperature, which lessens the influence of CO emission by the reaction of H and CH_3 radicals. At 6 bar IMEP, the influence of those radicals' oxidation at escalated temperatures might occur besides a reduced CO oxidation to CO_2, causing escalated emissions for 60 and 70% biogas portion.

Because the cooling effect of increasing CO_2 proportion or recombination of CH_3 radicals hindered the role of oxidized H and CH_3 at the elevated temperature, the CO emission dramatically decreases at 6.5 bar IMEP. The CO emissions patterns are similar for 35 and 45% CO_2 at various loads, as illustrated in Fig. 7c and Fig. 7d. However, radicals oxidation's impact was less pronounced with 35% CO_2 content leading to the lowest emission of 0.104% at 40% biogas fraction and 6.5 bar IMEP; thus, operating at such conditions could be less detrimental to human health. The lowest value is still higher than the minimum standard by 57.16%. These findings support the work of other studies in this area (Ambarita, 2017; Wang et al., 2016).

3.2.1.2. Optimized envirnmental CO emission prediction. The response CO emission was modeled to predict, analyze, and strategically determine the optimum input condition for minimized trade-offs, thereby reducing their environmental impacts. Table 6 provides an overview of the analysis of variance (ANOVA) for the outcome of the quadratic model of the CO emission. The ANOVA indicates a significant model with an insignificant lack of fit. Table 6 shows that the CO model has a significant F-value of 15.56 and there is a 0.09% possibility that noise could cause an F-value this high. The variables and the importance of the model were analyzed at a confidence level of 5% (P<0.05). The factors A, C, AC, A^2, and C^2 are statistically significant, as shown in Table 6, however, the other elements are not significant due to probabilities greater than 0.05. This finding indicates that the biogas proportion and engine load have a significant impact on CO emissions. On the other hand, elevated CO_2 content and the combination of factors have negligible effects on CO emissions, but the second-order impact of engine load and CO_2 content was statistically significant. The lack of fit term shows the likelihood of the expected value disagreeing with the actual value, indicating the model's goodness (Zou et al., 2019). A score larger than 0.05 therefore indicates that the equation is empirically appropriate. Also, a P-value of 0.2413 indicates that the model equation is acceptable. The finally developed model for CO emission in a basic form is offered in Eq. 4. The correlation coefficient (R^2) defines the quality and adequacy of the developed model; thus, for a good model, an R^2 value closed to one (1) is desirable with a required assurance of reasonable agreement with adjusted R^2. The adjusted R^2 indicates the effect of certain modifications on the actual R^2 for the number of predictors. Besides, the predicted R^2 measures the degree of diversity in the results of the suggested model. Table 7 demonstrates that the model accurately correlates 93.96% of experimental CO emission findings with the data's less aberrant elements. The model's low standard deviation (SD) value suggests a good correlation with experimental results, and its adequate precision (AP) of 13.92, which is greater than 4, confirms its suitability for the design space.

$$E_{CO} = -3.269 + 1.272A - 0.0118B - 0.00893C + 0.000064BC - 0.105A^2 + 0.00012B^2 + 0.000071C^2 \quad (4)$$

The developed model's two-dimensional (2D) contour plot reveals an excellent interactive effect between biogas fraction and CO_2 content, with semi-elliptical contour lines at 5.5 bar IMEP (Fig. 7a). Similar contour inclination appears at other loads, though the contour colors indicate apparent variabilities across the loads, as shown in Fig. 9b and Fig. 9c. The contour region in bluish color representing the lower CO emission appears in Fig. 9a. As observed, low CO emissions are dominant in high CO_2 and low biogas fraction region. Similarly, the contour region in reddish color representing the high CO emission dominantly occupies Fig. 9b, with more concentration around the upper limit of biogas fraction. The results correlate with the experimental outcome depicted in Fig. 7.

A 3D response curve was generated to examine the impact of independent factors on CO emission, demonstrating that increasing the biogas proportion enhanced CO emission (Fig. 8). Simultaneously, engine load resulted in peak emission at midway (6 bar IMEP), as established in Fig. 10a and similarly observed in Fig. 7b, Fig. 7c, and Fig. 7d. Fig. 10b shows decreased CO emission pattern with increased CO_2

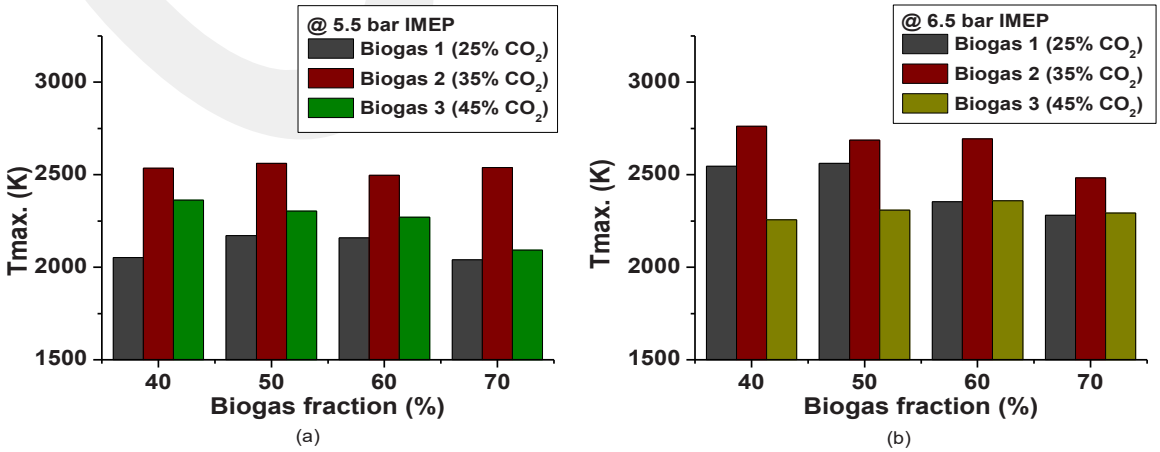

Fig. 8. Tmax at different fractions and CO_2 contents (a) 5.5 bar IMEP and (b) 6.5 bar IMEP.

Table 6
ANOVA for the response CO emission model.

Source	Sum of Squares	Degree of freedom (DF)	Mean Square	F-Value	p-value (Prob> F)	Remarks
Model	7.17E-03	7	1.02E-03	15.56	0.0009	significant
A-Engine load	5.63E-04	1	5.63E-04	8.56	0.0222	
B-CO_2 content	3.09E-04	1	3.09E-04	4.69	0.0671	
C-Biogas fraction	2.77E-03	1	2.77E-03	42.02	0.0003	
BC	1.63E-04	1	1.63E-04	2.47	0.16	
A^2	2.53E-03	1	2.53E-03	38.37	0.0004	
B^2	4.13E-04	1	4.13E-04	6.28	0.0407	
C^2	1.88E-04	1	1.88E-04	2.85	0.135	
Residual	4.61E-04	7	6.58E-05			
Lack of Fit	4.13E-04	5	8.25E-05	3.43	0.2413	insignificant
Pure Error	4.82E-05	2	2.41E-05			
Cor Total	7.63E-03	14				

Table 7
CO emission model validation for the intake regime.

Response	SD	Mean	R^2	Adjusted R^2	Predicted R^2	AP
CO	0.0081	0.16	0.9396	0.8792	0.5205	13.92
UHC	5.73	192.52	0.9951	0.9908	0.9746	49.398
NOx	0.13	3.75	0.9977	0.9935	0.9642	48.044
PM	1.00	17.37	0.9854	0.9679	0.7160	24.97

content, with biogas fraction being the most influential independent variable causing increased CO emission, while elevated CO_2 influences reduced emission. Therefore, increasing CO_2 content in biogas during combustion reduces toxic pollutants and CO emission risk, potentially causing O_2 displacement from lung haemoglobin.

3.2.2. *Effects biogas intake composition on UHC emission attributes*

3.2.2.1. Environmental UHC emission interpretation using kinetic mechanism. Fig. 11a demonstrates that UHC emission increases with biogas fraction over diluent CO_2 ratios at 5.5 bar IMEP. This is due to increased combustible CH_4 and non-combustible CO_2 in the mixture, inhibiting combustion while increasing UHC. Other factors include reduced in-cylinder temperature or more fuel trapped in crevices (Imtenan et al., 2014; Lim and Reitz, 2014; Wissink and Reitz, 2015). Kinetically, the low temperature leading to more UHC emission may also be attributed to CH_3 radicals recombination, which inhibits the combustion and causes UHC emission as depicted in Eq. 5 (Fischer and Jiang, 2015). Also, further recombination terminate the chain branching, Eq. 6 (Westbrook, 2000), likely resulting to more emission. The primary ignition feature involves the accumulation of hydrogen peroxide (H_2O_2), which decomposes at a certain temperature (Eq. 7 and Eq. 8), consuming fuel (Eq. 9) (Ebrahimi et al., 2018; Westbrook, 2000), thus, poor decomposition increases UHC emissions. Increased CO_2 content in biogas fractions reduces UHC emissions, which in turn reduces explosive substances. An increase in CO_2 content from 25% to 45% reduces UHC emissions by 58.69% on average for different biogas components. The study discovered that raising the biogas fraction from 40% to 70% increases UHC emissions by 54.78% on average.

$$2CH_3 + M \rightarrow C_2H_6 + M \quad (5)$$

$$CH_3 + CH_3 \rightarrow C_2H_6 \quad (6)$$

$$RH + HO_2 \rightarrow R + H_2O_2 \quad (7)$$

$$HO_2 + HO_2 \rightarrow H_2O_2 + O_2 \quad (8)$$

$$H_2O_2 + M \rightarrow OH + OH + M \quad (9)$$

For 25% CO_2, extending the load further indicates a similar UHC emission pattern, as depicted in Fig. 11b. Similar attributes appear for other CO_2 ratios shown in Fig. 11c and Fig. 11d. Running the engine at 6.5 bar IMEP reduces UHC emissions across CO_2 contents and biogas

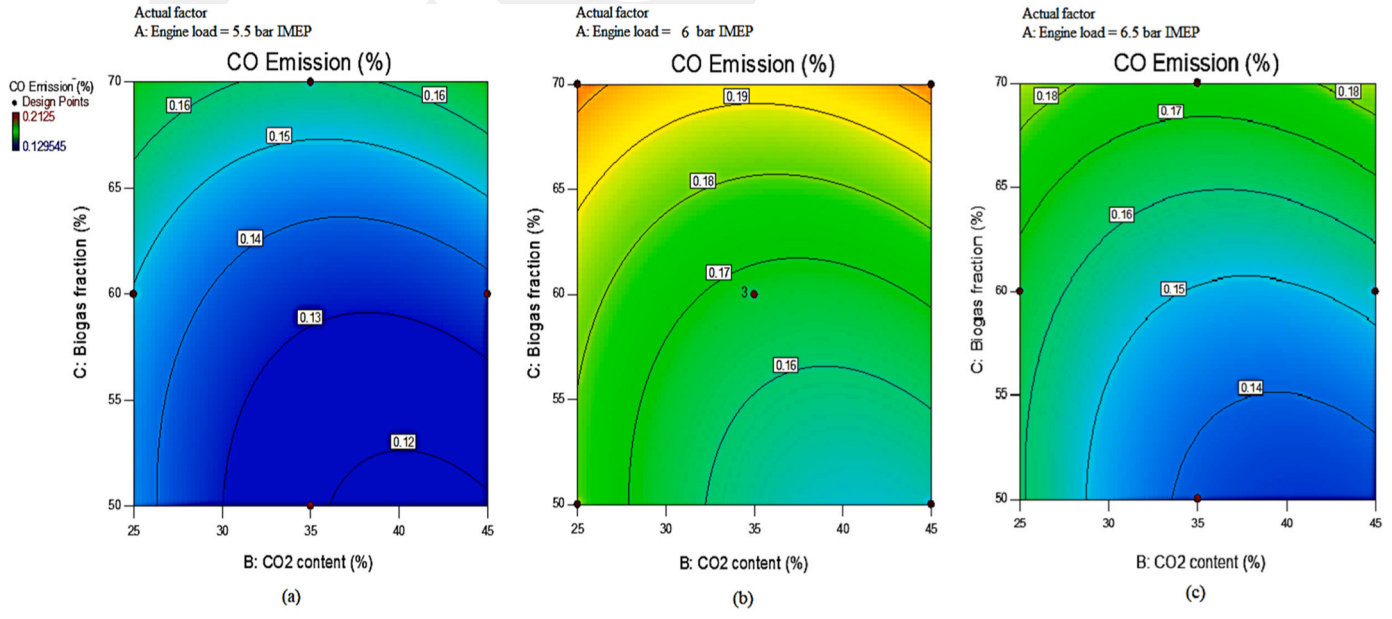

Fig. 9. 2D contour diagrams for CO emission at (a) 5.5 bar, (b) 6 bar, and (c) 6.5 bar IMEP.

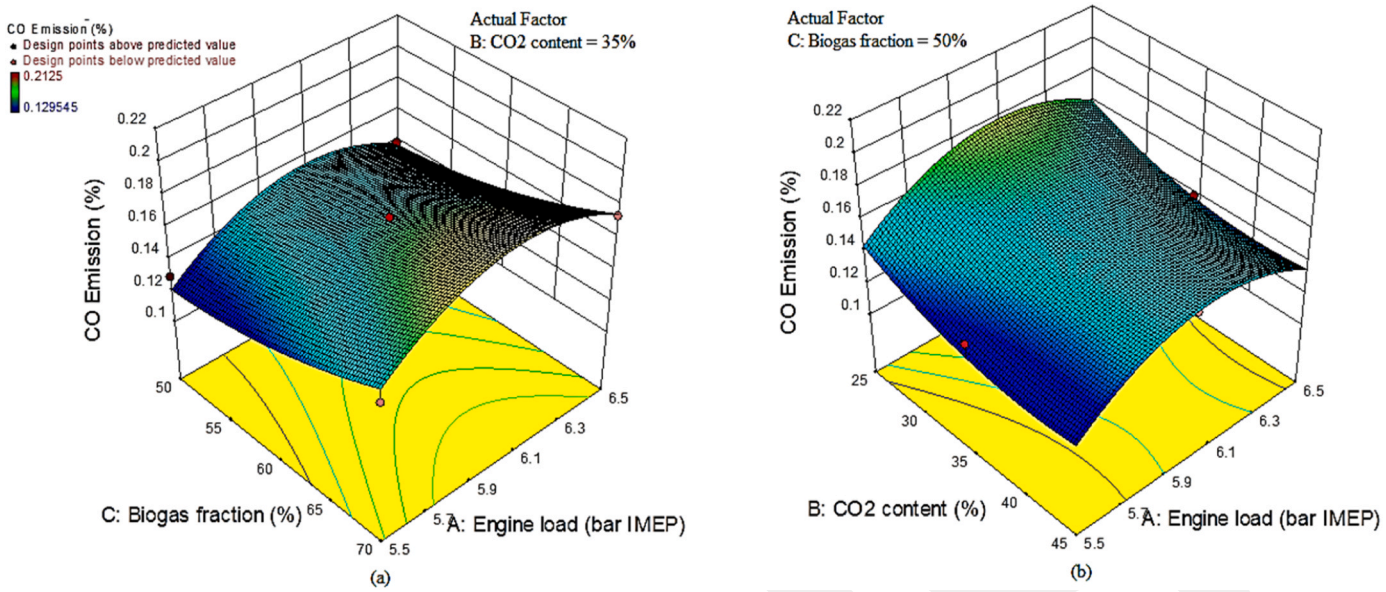

Fig. 10. 3D contour diagrams for the CO emission at (a) 35% CO_2 and (b) 50% biogas fraction.

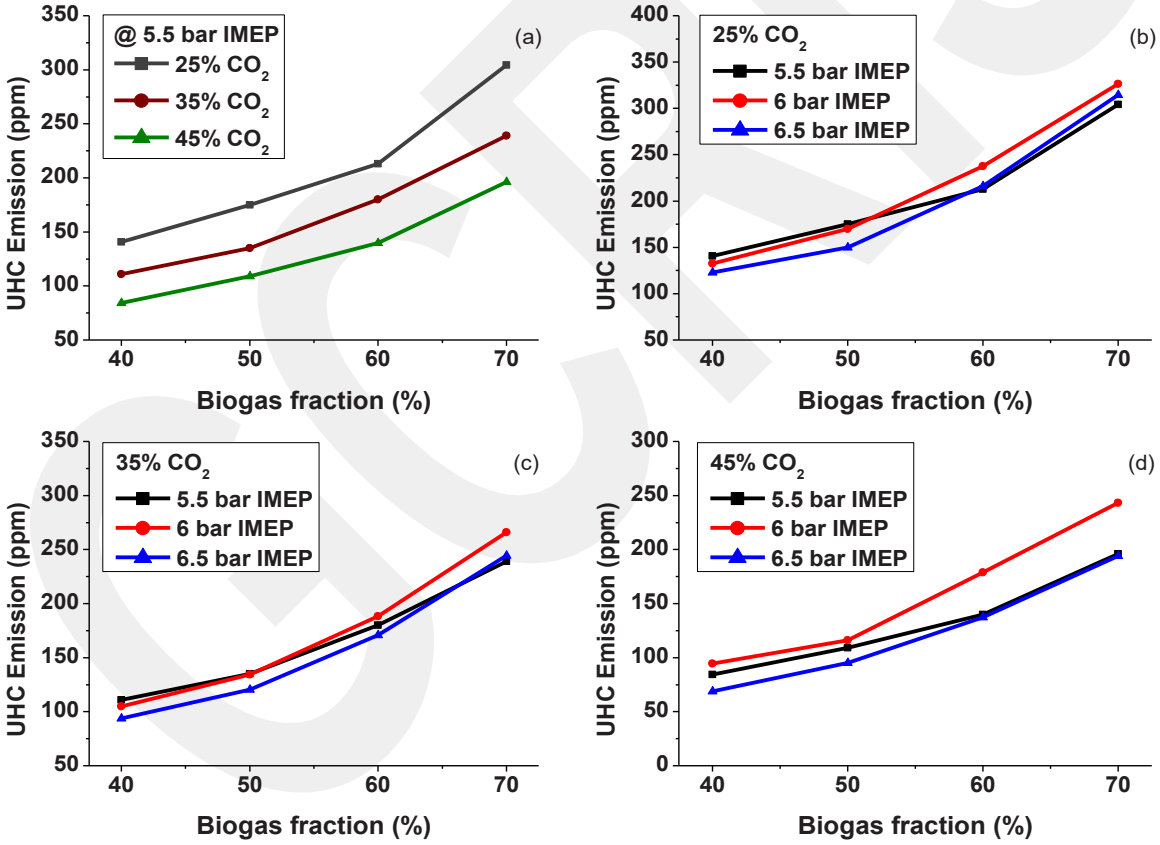

Fig. 11. UHC emission (a) 5.5 bar IMEP, (b) 25% CO_2, (c) 35% CO_2, and (d) 45% CO_2 for the loads.

fractions, lowering photochemical smog and greenhouse gasses in the atmosphere, probably due to greater temperatures produced at this temperature (Fig. 8a and Fig. 8b). The lowest UHC emission of 68.94 ppm was recorded at a 40% fraction and 45% CO_2, significantly lower than the minimum regulatory limit and represents a safer working environmental condition. These findings broadly support the work of other studies in this area (Ambarita, 2017; X. Wang et al., 2016).

3.2.2.2. Optimized envirnmental UHC emission prediction. The finally developed model for UHC emission in a basic form is offered in Eq. (10). Table 7 depicts the models' validation parameters for the intake regime. Thus, it was found suitable to navigate the design space. In comparison to the actual result, a graphical plot of the predicted findings in a 2D contour is shown in Fig. 12 to investigate the combined impact of the parameters on UHC emission. The contour lines in Fig. 12a unveils an apparent interactive effect between biogas fraction and CO_2 content,

having shown semi-elliptical curves. Similar contour inclination appears at other loads with little variabilities across the loads, as shown in Fig. 12b and Fig. 12c. The bluish color in the maps represents the low UHC emission area, while the reddish color depicts the high UHC region for all the loads. Reduced UHC emissions appear in the context of elevated CO_2 and low fraction. In contrast, the high UHC emission was predominant in the opposite area. Importantly, it can be inferred from the prediction results that no trade-off occurs between CO and UHC emissions that is advantageous in minimizing the environmental and health impacts, as illustrated in Fig. 9 and Fig. 12.

$$E_{UHC} = -2636.5 + 1173.89A - 12.95B - 19.11C - 98A^2 + 0.128B^2 + 0.209C^2 \quad (10)$$

The study found a significant increase in UHC emission with increased biogas fraction, but predicted a high emission trend at mid-load for 35% CO_2 content (Fig. 13a). Contrarily, Fig. 13b depicts a decreased UHC emission as the CO_2 content increases. Although the UHC emission was found to elevate at mid-load, model Eq. 10 predicts that it generally has insignificant positive impacts on the reduced emission. The biogas fraction is the primary independent variable contributing to higher UHC emissions, while rising CO_2 levels lower it.

3.2.3. Effects biogas intake composition on NOx emission attributes

3.2.3.1. Environmental NOx emission interpretation using kinetic mechanism. Analyzing NOx emissions is critical for understanding the trade-off between emissions and the environmental consequences of high CO_2 content. Increased biogas proportion at 5.5 bar IMEP results in lower NOx emissions due to lower cylinder temperature and nitrogen-oxygen bond formation (Fig. 14a) (Isik, Hüseyin, 2016). Except for 70%, adding 25% CO_2 increases NOx emissions across the biogas portion due to higher H and CH_3 oxidation processes in lean settings (Eq. 1 and Eq. 2) (Fischer and Jiang, 2015). Fig. 8a indicates that lower temperatures and enhanced pressure-induced N_2 oxidation, on the other hand, might result in larger NOx emissions (Eq. 11 and Eq. 12) (Fischer and Jiang, 2015). Variabilities in kinetics reactions involving N_2 caused by fluctuating cylinder temperature and pressure result in variable NOx emission patterns due to increasing CO_2 content at various biogas fractions, as illustrated in Fig. 14a. According to the study, increasing the biogas portion from 40% to 70% reduces NOx emissions by 66.39% on average, while increasing the CO_2 content from 25% to 45% reduces emissions by 35.95%. The lowest emission was 3 ppm at a 70% fraction across the CO_2 ratios, which was much lower than the standard limit. These findings broadly support the work of other studies in this area (Rahnama et al., 2017; X. Wang et al., 2016).

$$O + N_2 \rightarrow N + NO \quad (11)$$

$$O + N_2 + M \rightarrow N_2O + M \quad (12)$$

Fig. 14b demonstrates a continuous minor increase in NOx emission at 6 bar IMEP and 25% CO_2, with increased biogas proportion, while raising the CO_2 to 35% and 45% exhibit same NOx emission patterns, as shown in Fig. 14c and Fig. 14d. Disparities in load levels are evident, with 25% CO_2 indicating the lowest NOx emission at most biogas fractions for 6.5 bar IMEP, possibly due to increased cylinder temperature (Fig. 8a and Fig. 8b). As illustrated in Fig. 7, Fig. 11, and Fig. 14, increasing biogas fractions led to an alarming NOx trade-off with CO and UHC emissions across the CO_2 contents and loads. Importantly, increasing the CO_2 ratios mitigates the emissions trade-off across the biogas fractions when run at 5.5 bar IMEP, as established in Fig. 7a, Fig. 11a, and Fig. 14a. These trends signify that although photochemical smog risk might be lowered due to reduced UHC emission, increased NOx might contrarily promote it besides increased acid rain and degraded stratospheric ozone. Hence, the need for optimization to properly manage the trade-off among those emission parameters.

3.2.4. Optimized envirnmental NOx emission prediction

The final developed model for NOx emission in its basic form is offered in Eq. (13) along with validation parameters in Table 7, confirming its suitability for exploring the conceptual domain. Despite CO_2 concentration being low at 5.5 bar IMEP, the model's 2D contour diagram displays a strong interaction between biogas fraction and CO_2 content, with elliptical paths (Fig. 15a). Similar contour inclination appears at other loads with significant variabilities across, as shown in Figs. 13b and 13c. The bluish color representing the lower NOx emission is predominantly shown at low load, as depicted in Fig. 15a. Increasing the load unveils an element of increased NOx emission with an increased concentration towards the lower biogas fraction region, as shown in Fig. 15b. In Fig. 15c, the reddish color depicts the high NOx region with

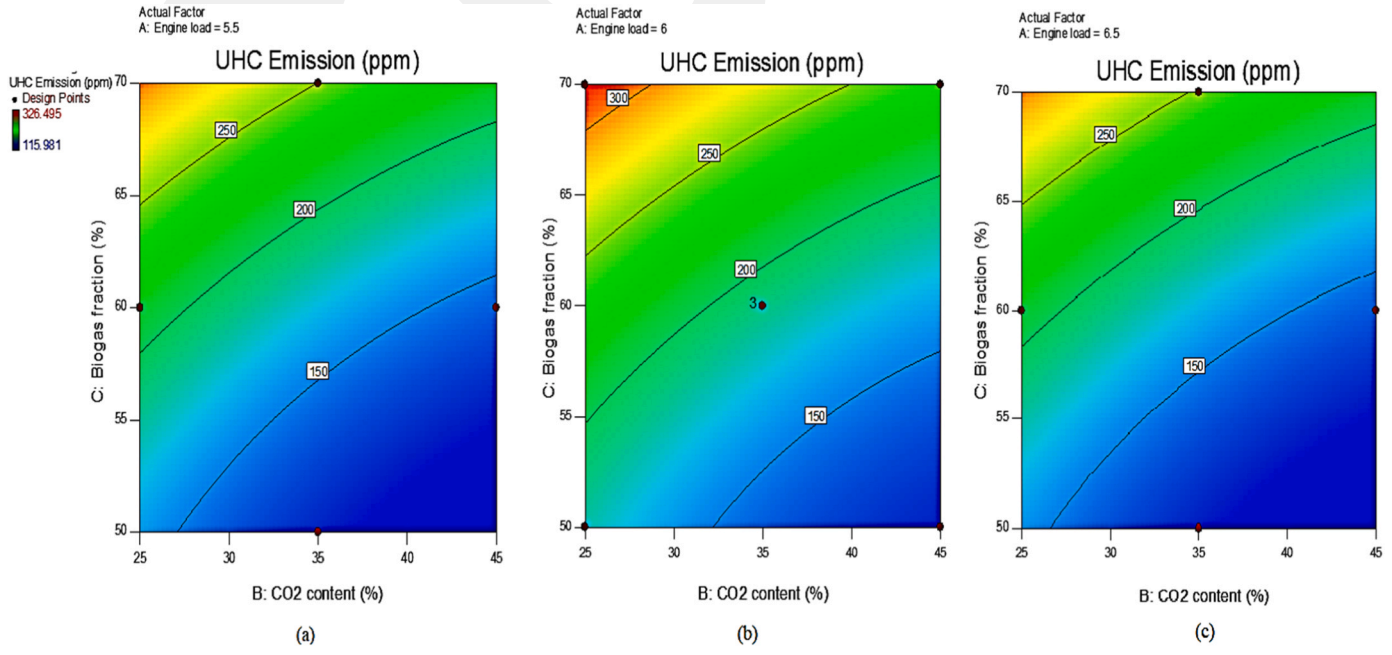

Fig. 12. 2D contour diagrams for UHC emission at (a) 5.5 bar, (b) 6 bar, and (c) 6.5 bar IMEP.

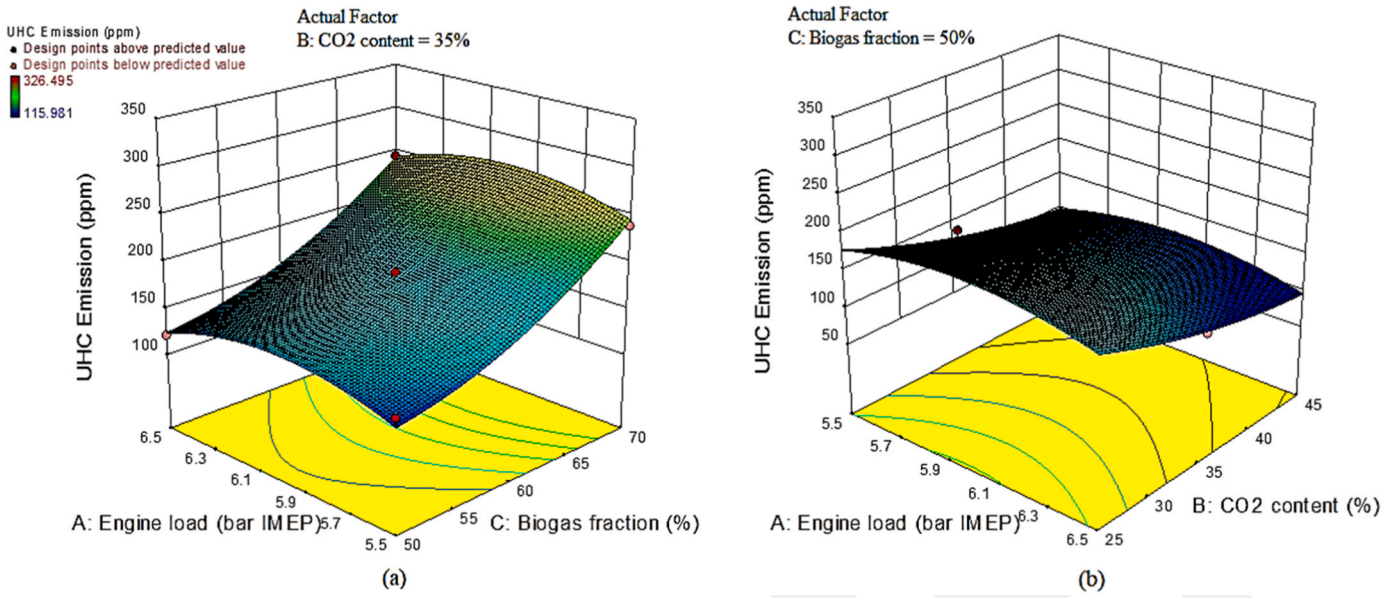

Fig. 13. 3D contour diagrams for UHC (a) 35% CO_2, and (b) 50% biogas fraction.

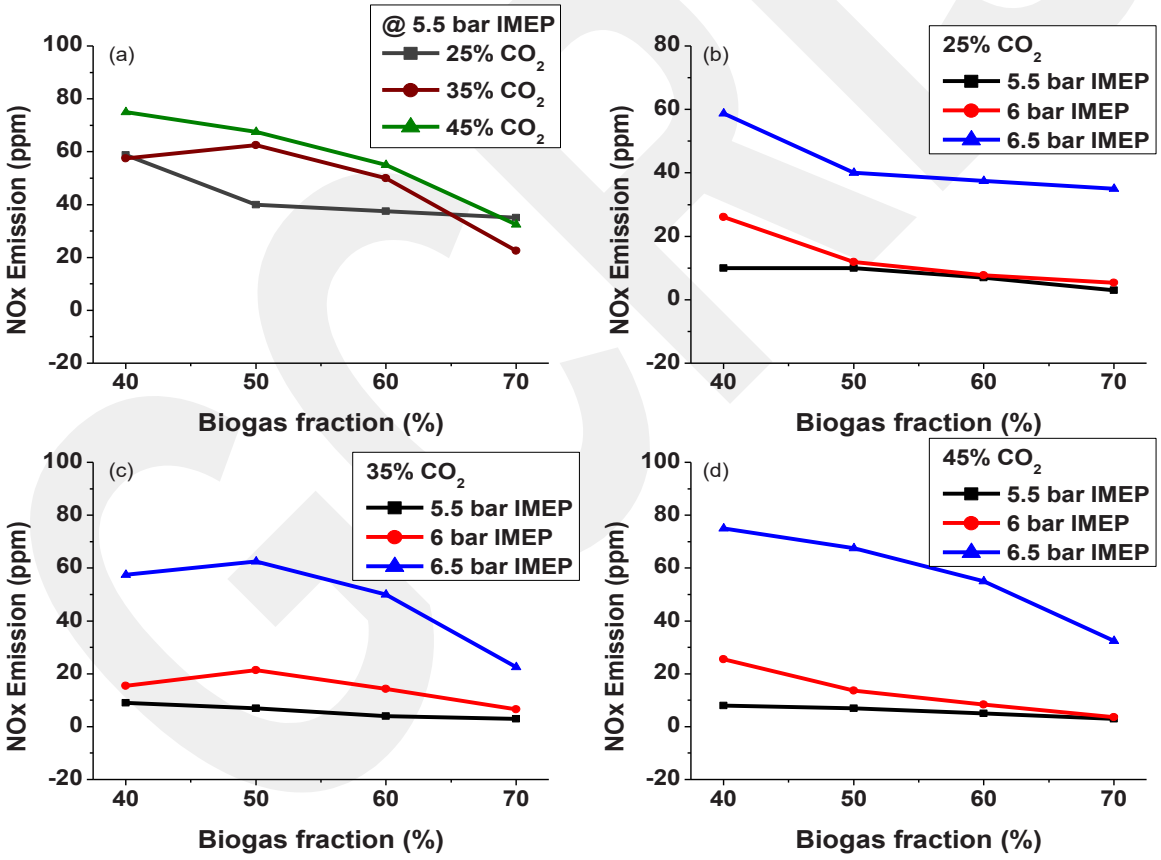

Fig. 14. NOx emission at (a) 5.5 bar IMEP, (b) 25% CO_2, (c) 35% CO_2, and (d) 45% CO_2.

the highest concentration at elevated CO_2 in connivance with low biogas fraction at 6.5 bar IMEP. Fig. 9, Fig. 12, and Fig. 15 show no trade-off between CO, UHC, and NOx emissions, particularly at low biogas fraction regions across the CO_2 ratios under 5.5–6 bar IMEP. It is because those areas fall within the bluish color mapping in the figures. However, a severe trade-off in those regions was predicted at 6.5 bar IMEP shown in Fig. 9c, Fig. 12c, and Fig. 15c. Therefore, high CO_2 content and low biogas fraction have great trade-off reduction ability, especially at moderate loads that reduce environmental and health risk. The 3D plot shows that NOx emission increases dramatically with increased load, as established in Fig. 16a. The figure further unveils that an increased biogas fraction lowers the NOx emission, especially at 6.5 bar IMEP for the 35% CO_2 ratio, as similarly observed with the other CO_2 rates. According to Fig. 16b, a high CO_2 content elevates the NOx emission,

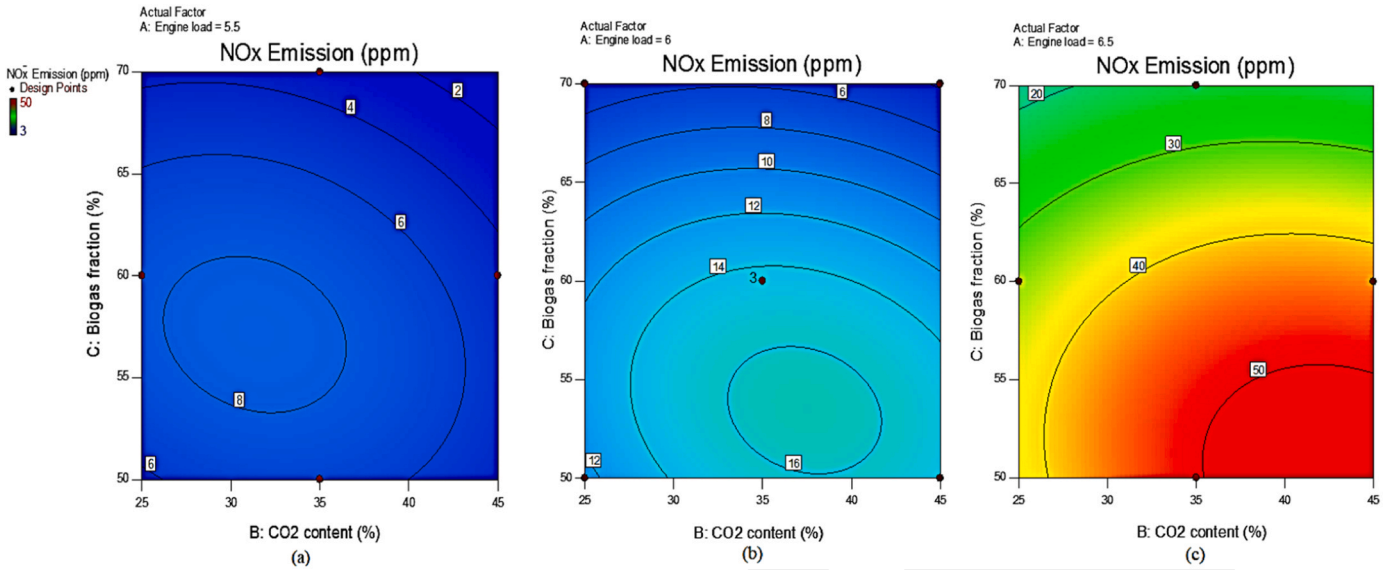

Fig. 15. 2D contour diagrams for NOx at (a) 5.5 bar, (b) 6 bar, and (c) 6.5 bar IMEP.

especially at 6.5 bar IMEP for the 50% fraction, similar to the other fractions. Accordingly, the notable factor producing increased NOx emission is engine load, while biogas fraction influences lower emission.

$$(E_{NOx})^{\frac{1}{2}} = +70.04 - 36.13A - 0.079B + 1.15C + 0.071AB - 0.071AC - 0.0017BC + 3.47A^2 - 0.0035B^2 - 0.0062C^2 \quad (13)$$

3.2.5. *Effects biogas intake composition on PM emission attributes*

Fig. 17a depicts that PM emission drops at 50% fraction and increases gradually from 60% to 70% biogas for all the CO_2 contents except 45% at 5.5 bar IMEP. According to (Benajes et al., 2018), utilizing less diesel with improved timing of injection increases fuel blending, resulting in lower particles of soot at a 50% proportion. This pattern shows that an ideal mixture at a 50% proportion could occur, leading to low PM emitted, but increases with increased CO_2 content over biogas fraction, potentially increasing carbon particle rate. Increasing the CO_2 content from 25% to 45% increases average PM emission by 60.19%, but increasing the biogas portion also strengthens the PM emission compromise with CO and UHC at 5.5 bar IMEP. At 5.5 bar IMEP, the lowest PM emission of 3 ppm was reported for 25% CO_2 with a 50% portion. Extending engine load to 6 bar IMEP for 25% CO_2 shows an opposing PM emission trend (Fig. 17b), which drops gradually with increased biogas portion due to early injection time that lowers soot formation (Benajes et al., 2018). This trend implies that better mixing happens at a fraction of 70%, causing less PM emission. In contrast, a case of 6.5 bar IMEP demonstrates a pattern closed to occurance of 5.5 bar IMEP, causing better mixing at 60% biogas fraction. Fig. 17c shows that a case of 35% CO_2 follows the trend of 25% for all the loads vividly, unlike 45% that shows reverse trends at 5.5 and 6 bar IMEP illustrated in Fig. 17d. These trends also indicate the need for optimization to determine the optimum condition for minimal risk of increased oxidative stress.

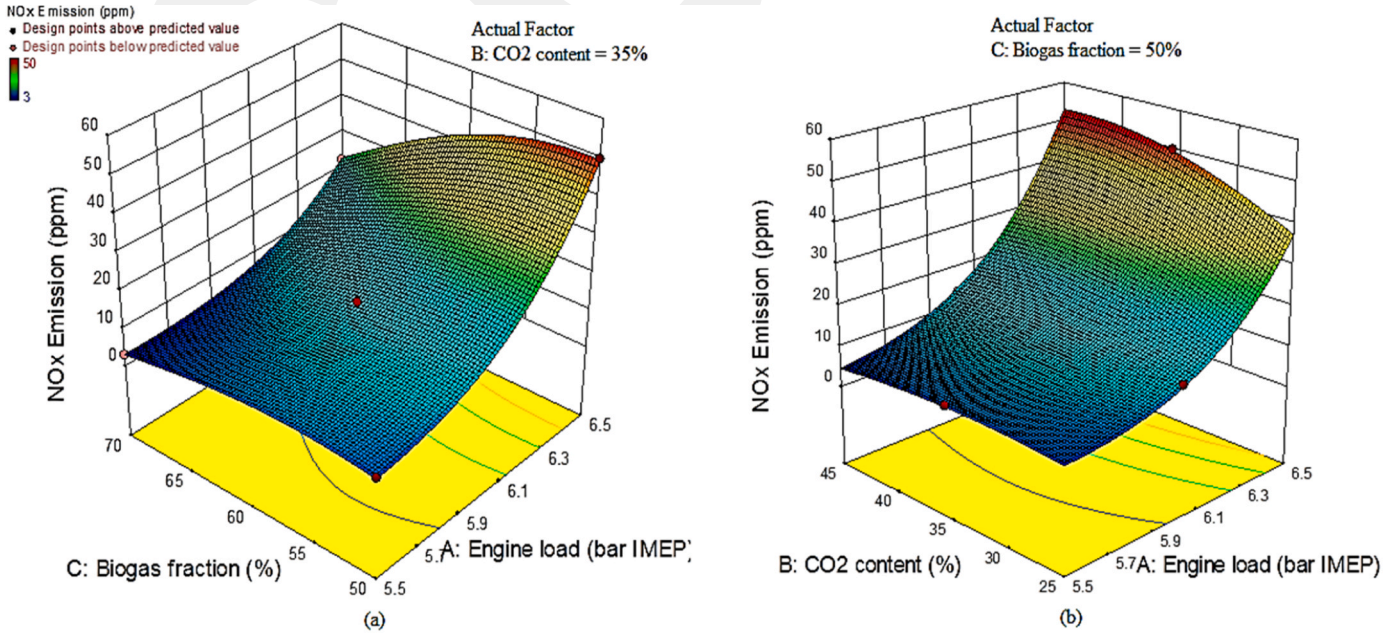

Fig. 16. 3D contour diagrams for the NOx emission at (a) 50% biogas fraction, and (b) 35% CO_2 ratio.

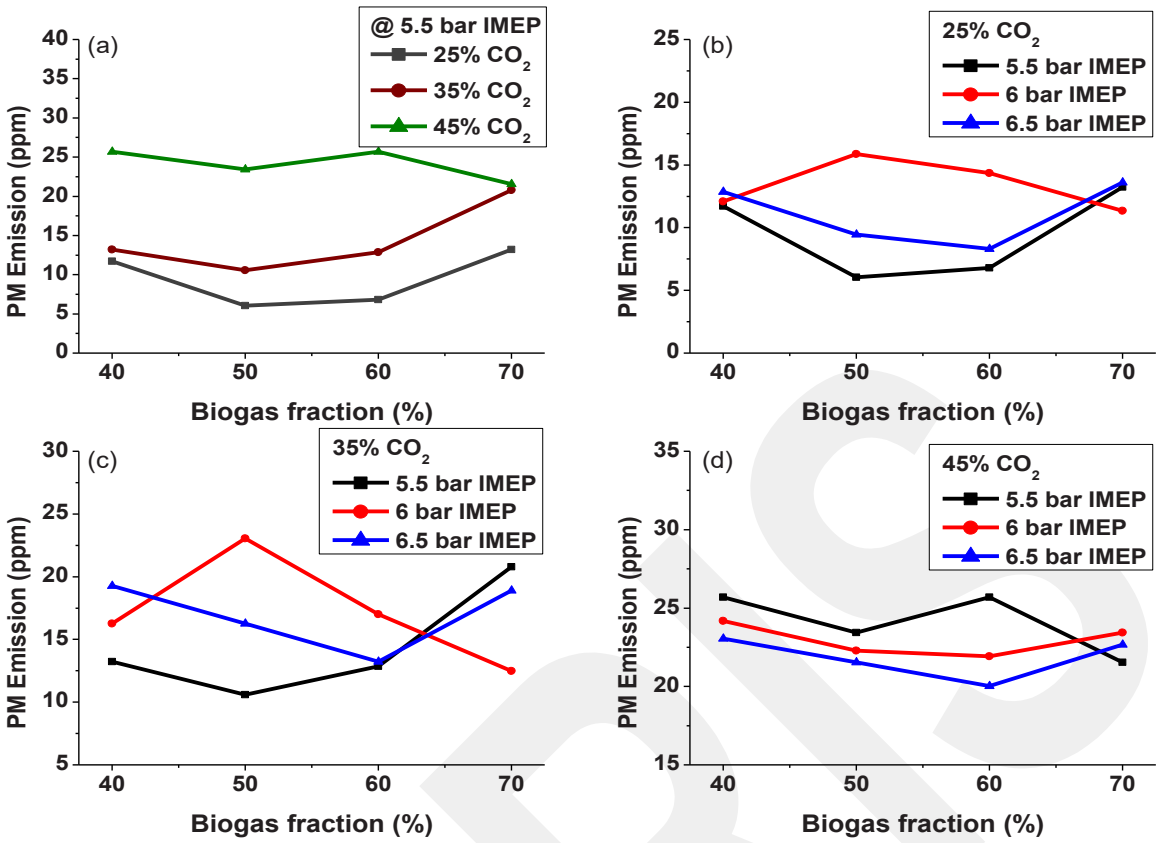

Fig. 17. PM emission at (a) 5.5 bar IMEP, (b) 25% CO_2, (c) 35% CO_2, and (d) 45% CO_2.

3.2.5.1. Optimized environmental PM emission prediction. The final developed model for NOx emission in its basic form is offered in Eq. (14) along with validation parameters in Table 7, confirming its suitability for exploring the conceptual domain. The model's outcome is presented in a 2D map, revealing a significant interaction between biogas fraction and CO_2 content, as shown in Fig. 18a, with diagonal mappings at a 5.5 bar IMEP. Similar contour inclination appears at other loads with significant variabilities, though it has statistically insignificant effects, as shown in Fig. 16b and Fig. 18c. The bluish contour region shows lower PM emission, while reddish indicates high PM. At 6.5 bar IMEP, a slight variable with modest PM emission, indicated by a light bluish to greenish shade, can be noticed (Fig. 18c). Fig. 9, Fig. 12, Fig. 15, and Fig. 18 show no trade-off between CO, UHC, NOx, and PM emissions in the low biogas fraction and low CO_2 area at 5.5–6 bar IMEP, suggesting a safer setting for lower environmental risk. Therefore, using moderate CO_2 content and low biogas fraction has great trade-off reduction

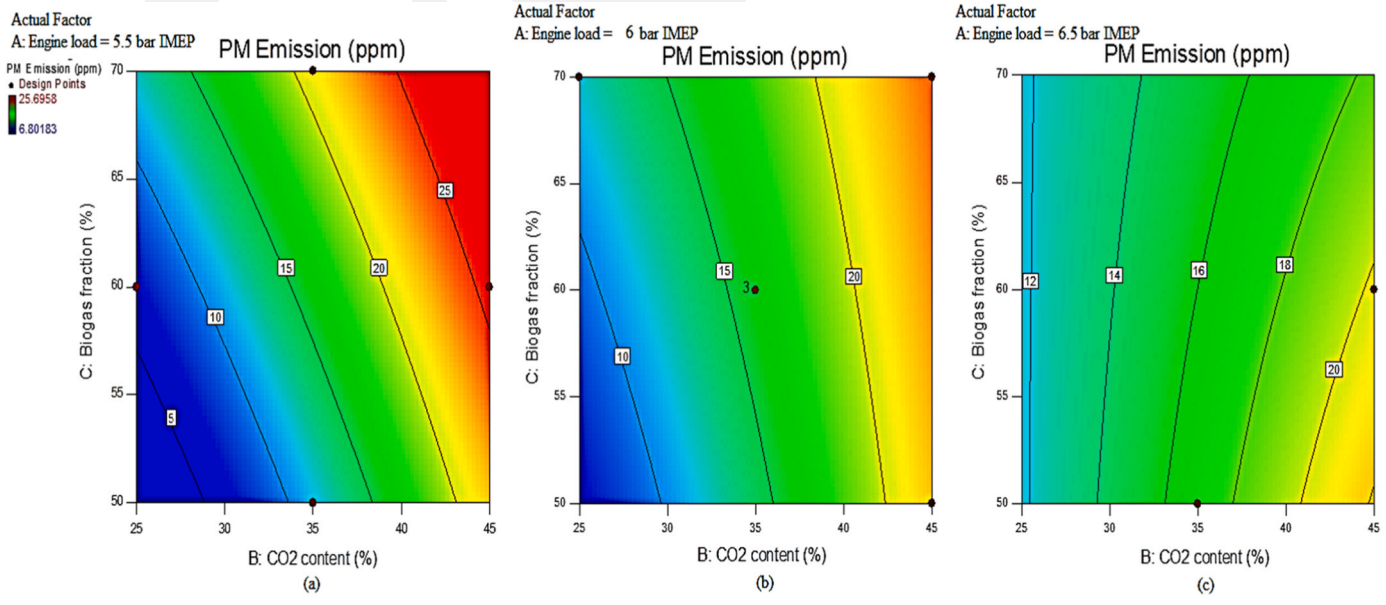

Fig. 18. 2D contour diagrams for the PM emission at (a) 5.5 bar, (b) 6 bar, and (c) 6.5 bar IMEP.

ability, especially 5.5–6 bar IMEP.

$$E_{PM} = -355.38 + 52.64A + 4.458B + 3.947C - 0.532BC - 0.570AC - 0.0096BC \quad (14)$$

The 3D response graph presented in Fig. 19a shows that at a biogas portion of 60%, PM emission grows dramatically with rising CO_2 content. Similarly, the PM emission increases with the increased engine load at the low CO_2 range under the same biogas fraction but indicates a contrary trend at high CO_2. Fig. 19b depicts increasing PM emission with 45% CO_2 biogas concentration, whereas emission remains constant at low biogas fractions but decreases at high fractions. The model predicts that as load increases, PM emissions decreases insignificantly, with CO_2 concentration and biogas fraction being the most notable variables elevating PM.

3.2.6. *Optimization and models validation for the intake regime*

The quest to achieving reduced engine-out emissions prompts the search for desirable high CO_2 ratio, biogas fraction, and engine load using a multi-objective optimization technique. The optimization process identifies key variables for achieving set goals, enhancing RSM responses, and determining optimal input CO_2 ratio, biogas fraction, and load to minimize emissions based on certain criterion. The models achieved improved results, with a total desirability of 75.42%, as shown in Fig. 20a, with the optimal condition presented in a 3D diagram (Fig. 20b). Individually, a 100% desirability was attained for CO and UHC emissions because of the weight and importance, highly desired for this research. However, the optimum CO, UHC, NOx, and PM emissions for the premixed RCCI combustion are 0.119%, 117.3 ppm, 6.602 ppm, and 12.07 ppm at a load of 5.5 bar IMEP, 50% biogas fraction, and 35.586% CO_2 rate.

Some tests were conducted using optimized intake variables and two more different conditions to validate the optimization results' appropriateness and the whole output models. Eq. 15 was used to determine the relative errors for the experimental and predicted outcomes, as summarized in Table 8. It can be inferred based on the information in Table 8 that the expected and experimental results were in mutual agreement, having shown minor percentage errors. The positive errors imply that the observed outcomes are more significant than the predicted and vice versa.

$$Error \quad (\%) = \frac{Experimental \quad outcome - Predicted \quad outcome}{Experimental \quad outcome} * 100 \quad (15)$$

4. Conclusion

An exploratory analysis was carried out in a premixed RCCI mode on the effect of direct-injected fuels at different operational conditions and biogas containing elevated CO_2 at various rate and fractions. Using kinetic mechanisms, the effects of these parameters on emission occurrences were also predicted and analysed. This paper also pioneered the use of established kinetic mechanisms along with multi-objective optimization to analyze emissions occurrence and trade-offs.

The result showed that operating the engine at high engine load reduced UHC emissions, while engine speeds significantly reduced CO and NOx emissions with increasing UHC regardless of HRF used. Except for low-level loads, diesel-biogas reduces NOx emissions and outperforms B5-biogas in decreasing CO and UHC emissions at lower speeds. When compared to 2000 rpm, CO emission drops by 25–31.58% at 1600 rpm, while UHC emissions rise by 35.24% on average across all the loads. The CO emission of both reactivity fuels happened to be significantly higher than the standard limit, while UHC and NOx were substantially lower.

The research work conclude that biogas fraction was the most influential independent variable causing increased CO and UHC emissions while reduced by the elevated CO_2 influence. The engine load was the most influential variable causing increased NOx emission but biogas fraction reduces it meanwhile high CO_2 content as well as biogas fraction increases PM emission. Finally, the optimum CO, UHC, NOx, and PM emissions for the premixed RCCI combustion are 0.119%, 117.3 ppm, 6.602 ppm, and 12.07 ppm at a load of 5.5 bar IMEP, 50% biogas fraction, and 35.586% CO_2 rate.

Consequently, running the single-cylinder RCCI engine with direct-injected diesel co-powered in equal proportion with high-CO_2 biogas significantly reduces the emissions trade-off, minimizing the environmental consequences of those emissions. The work provides more insight into emissions and their trade-off as serious setbacks in RCCI combustion that could be reconciled through port injection of biogas containing high CO_2. Consequently, the study suggested that more

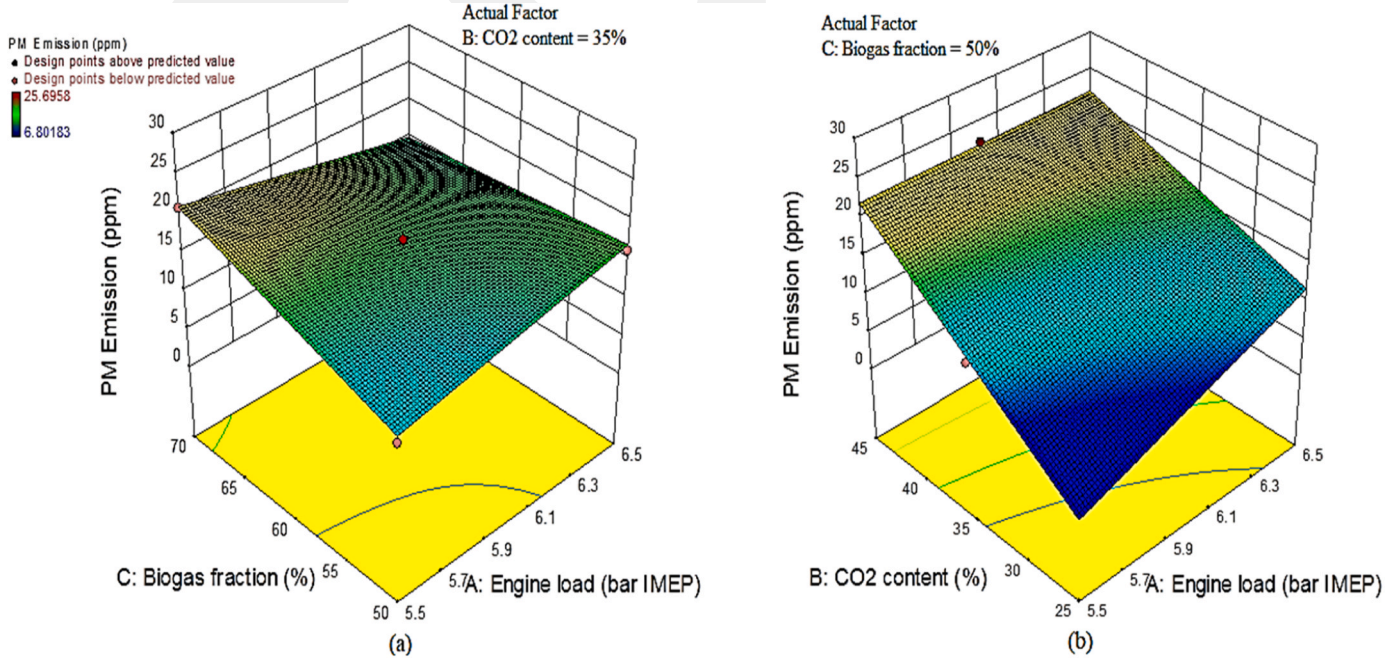

Fig. 19. 3D contour diagrams for the PM emission at (a) 35% CO_2, and (b) 50% biogas fraction.

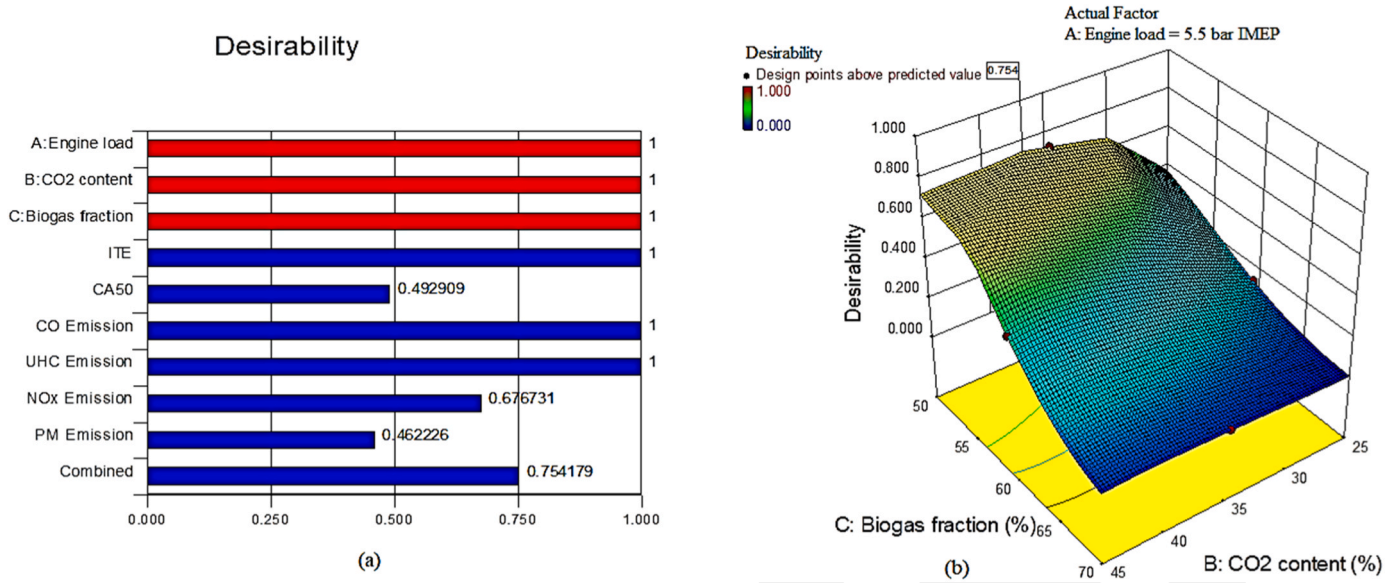

Fig. 20. (a) Desirability distribution and (b) desirable combination of the intake variables.

Table 8
Models verification for the intake regime.

Responses (intake)	Engine load	CO_2 content	Biogas fraction	Predicted results	Experimental results	Error (%)
CO Emission (%)	5.5	35.586	50	0.119	0.125	4.80
	6	35	60	0.167	0.163	-2.71
	6.5	45	60	0.154	0.151	-2.13
UHC Emission (ppm)	5.5	35.586	50	117.3	125.0	6.18
	6	35	60	188.3	187.4	-0.45
	6.5	45	60	134.9	137.2	1.69
NOx Emission (ppm)	5.5	35.586	50	6.602	7.010	5.82
	6	35	60	13.66	14.22	3.91
	6.5	45	60	46.26	44.10	-4.89
PM Emission (ppm)	5.5	35.586	50	12.07	12.85	6.07
	6	35	60	16.09	17.17	6.27
	6.5	45	60	20.24	20.02	-1.08

research be conducted into the impacts of high-CO2 biogas which comprises certain constituents of other gases to better resemble raw biogas.

Funding

This work was supported by Malaysia's Petroleum Research Fund (PRF) Grant (Cost Centre: 0153AB-A34) and Nigeria's National Research Fund (NRF), TETFund 2021 (Project Code: TETF/ES/DR&D-CE/NRF2021/SETI/WAS/00034/VOL.1).

CRediT authorship contribution statement

Ibrahim B. Dalha; conceptualization, methodology, investigation and writing, Mior A. Said; funding acquisition, supervision, review, and editing, Kemal Koca; funding, review, and editing, Aminu D. Rafindadi; project administration and review.

Declaration of Competing Interest

The authors declare that they have no known competing financial interests or personal relationships that could have appeared to influence the work reported in this paper.

Acknowledgments

The authors gratefully acknowledged the support provided by the Centre for Automotive Research and Electric Mobility (CAREM), Universiti Teknologi PETRONAS (UTP), Malaysia, Bio-Resources Laboratory, Ahmadu Bello University (ABU), Nigeria, and Abdullah Gul University (AGU), Turkey in undertaking this research, its write-up, and publication.

References

Ambarita, H., 2017. Performance and emission characteristics of a small diesel engine run in dual-fuel (diesel-biogas) mode. Case Stud. Therm. Eng. 10, 179–191. https://doi.org/10.1016/j.csite.2017.06.003.

Russell, Armistead G., Atkinson, Roger, Bowling, Sue Ann, Colome, Steven D., Duan, Naihua, Gallagher, Gerald, Guensler, Randall l, Handy, Susan l, Hochgreb, Simone, Mohr, Sandra N., Pielke SR, Roger A., Springer, Karl J., R.W, 2002. The Ongoing Challenge of Managing Carbon Monoxide Pollution in Fairbanks, Alaska: Interim Report (2002). National Academy Press,, Washington, D.C.. https://doi.org/10.17226/10378

Barabad, M.L.M., Jung, W., Versoza, M.E., Kim, M., Ko, S., Park, D., Lee, K., 2018. Emission characteristics of particulate matter, volatile organic compounds, and trace elements from the combustion of coals in mongolia. Int. J. Environ. Res. Public Health 15. https://doi.org/10.3390/ijerph15081706.

Barik, D., Murugan, S., 2016. Experimental investigation on the behavior of a DI diesel engine fueled with raw biogas e diesel dual fuel at different injection timing. J. Energy Inst. 89, 373–388. https://doi.org/10.1016/j.joei.2015.03.002.

Benajes, J., García, A., Monsalve-Serrano, J., Lago Sari, R., 2018. Fuel consumption and engine-out emissions estimations of a light-duty engine running in dual-mode RCCI/CDC with different fuels and driving cycles. Energy 157, 19–30. https://doi.org/10.1016/j.energy.2018.05.144.

Benajes, J., Molina, S., García, A., Belarte, E., Vanvolsem, M., 2014. An investigation on RCCI combustion in a heavy duty diesel engine using in-cylinder blending of diesel and gasoline fuels. Appl. Therm. Eng. 63, 66–76. https://doi.org/10.1016/j.applthermaleng.2013.10.052.

Benajes, J., Molina, S., García, A., Monsalve-Serrano, J., 2015. Effects of direct injection timing and blending ratio on RCCI combustion with different low reactivity fuels. Energy Convers. Manag. 99, 193–209. https://doi.org/10.1016/j.enconman.2015.04.046.

Bora, B.J., Saha, U.K., 2016. Experimental evaluation of a rice bran biodiesel e biogas run dual fuel diesel engine at varying compression ratios. Renew. Energy 87, 782–790. https://doi.org/10.1016/j.renene.2015.11.002.

Borlaza, L.J.S., Cosep, E.M.R., Kim, S., Lee, K., Joo, H., Park, M., Bate, D., Cayetano, M. G., Park, K., 2018. Oxidative potential of fine ambient particles in various environments. Environ. Pollut. 243, 1679–1688. https://doi.org/10.1016/j.envpol.2018.09.074.

Bortel, I., Takáts, M., Diviš, M., 2017. Emissions and performance of diesel – natural gas dual-fuel engine operated with stoichiometric mixture. Fuel 208, 722–733. https://doi.org/10.1016/j.fuel.2017.07.057.

Dalha, Ibrahim B., Said, M.A., Abdul Karim, Z.A., Aziz, A.R.A., Firmansyah, Abidin, E.Z. Z., Ismael, M.A., 2020. Reactivity Controlled Compression Ignition: An Advanced Combustion Mode for Improved Energy Efficiency. Energy Efficiency in Mobility Systems. Springer,, pp. 101–126. https://doi.org/10.1007/978-981-15-0102-9_6.

Dalha, I.B., Said, M.A., Abdul, Z.A., El-adawy, M., 2021. Effects of port mixing and high carbon dioxide contents on power generation and emission characteristics of biogas-diesel RCCI combustion. Appl. Therm. Eng. 198, 117449 https://doi.org/10.1016/j.applthermaleng.2021.117449.

Dalha, I.B., Said, M.A., Karim, Z.A.A., Mohammed, S.E.D., 2022. Effects of high CO2Contents on the Biogas/Diesel RCCI combustion at full engine load. Evergreen 9, 49–55. https://doi.org/10.5109/4774216.

Dalha, Ibrahim, B., Said, M.A., Karim, Z.A.A., Salah, E.M., 2020. An experimental investigation on the influence of port injection at valve on combustion and emission characteristics of B5 / Biogas RCCI engine. Appl. Sci. 10, 1–25. https://doi.org/10.3390/app10020452.

Deshpande, N.V., Kale, N.W., Deshmukh, S.J., 2012. A study on biogas generation from Mahua (Madhuca indica) and Hingan (Balanites aegyaptiaca) oil seedcake. Energy Sustain. Dev. 16, 363–367. https://doi.org/10.1016/j.esd.2012.07.003.

Duic, N., Vujanovic, M., Krajac, G., 2016. Sustainable development of energy, water and environment systems for future energy technologies and concepts. Energy Convers. Manag. 125, 1–14. https://doi.org/10.1016/j.enconman.2016.08.050.

Ebrahimi, M., Jazayeri, S.A., 2019. Effect of hydrogen addition on RCCI combustion of a heavy duty diesel engine fueled with landfill gas and diesel oil. Int. J. Hydrog. Energy 44, 7607–7615. https://doi.org/10.1016/j.ijhydene.2019.02.010.

Ebrahimi, M., Najafi, M., Jazayeri, S.A., Mohammadzadeh, A.R., 2018. A detail simulation of reactivity controlled compression ignition combustion strategy in a heavy-duty diesel engine run on natural gas/diesel fuel. Int. J. Engine Res. 19, 774–789. https://doi.org/10.1177/1468087417730486.

Edwards, T.D., Wang, J.M., Hilker, N., Jeong, C.-H., Evans, G.J., 2021. Measurement of real-world roadway emission rates through a fitted dispersion model. Atmos. Pollut. Res. 12, 75–88. https://doi.org/10.1016/j.apr.2021.01.016.

Eklund, B., Anderson, E.P., Walker, B.L., Burrows, D.B., 1998. Characterization of landfill gas composition at the Fresh Kills municipal solid-waste landfill. Environ. Sci. Technol. 32, 2233–2237. https://doi.org/10.1021/es980004s.

El-Adawy, M., 2023. Effects of diesel-biodiesel fuel blends doped with zinc oxide nanoparticles on performance and combustion attributes of a diesel engine. Alex. Eng. J. 80, 269–281. https://doi.org/10.1016/j.aej.2023.08.060.

Firmansyah, A. Aziz, A., Heikal, M., Zainal A, E., 2017. Diesel/CNG Mixture Autoignition Control Using Fuel Composition and Injection Gap. Energies 10, 1639. https://doi.org/10.3390/en10101639.

Fischer, M., Jiang, X., 2015. An investigation of the chemical kinetics of biogas combustion. Fuel 150, 711–720. https://doi.org/10.1016/j.fuel.2015.01.085.

Gharehghani, A., Hosseini, R., Mirsalim, M., Jazayeri, S.A., 2015. An experimental study on reactivity controlled compression ignition engine fueled with biodiesel/natural gas. Energy 89, 558–567. https://doi.org/10.1016/j.energy.2015.06.014.

Gund, M.D., Tamboli, S.A., Mohite, V.R., 2017. Performance evaluation of single cylinder diesel engine in dual fuel mode with biogas as primary fuel and diesel and biodiesel as pilot fuel. Int. Res. J. Eng. Technol. 04, 1656–1660.

Gupta, S.K., Mittal, M., 2019. Effect of biogas composition variations on engine characteristics including operational limits of a spark-ignition engine. J. Eng. Gas. Turbines Power 141, 1–24. https://doi.org/10.1115/1.4044195.

Hopke, P.K., Hill, E.L., 2021. Health and charge benefits from decreasing PM2.5 concentrations in New York State: Effects of changing compositions. Atmos. Pollut. Res. 12, 47–53. https://doi.org/10.1016/j.apr.2021.01.018.

Hosseini, S.E., Wahid, M.A., 2013. Biogas utilization: experimental investigation on biogas flameless combustion in lab-scale furnace. Energy Convers. Manag. 74, 426–432. https://doi.org/10.1016/j.enconman.2013.06.026.

Imtenan, S., Varman, M., Masjuki, H.H., Kalam, M.A., Sajjad, H., Arbab, M.I., Fattah, I.M. R., 2014. Impact of low temperature combustion attaining strategies on diesel engine emissions for diesel and biodiesels: A review. Energy Convers. Manag. 80, 329–356. https://doi.org/10.1016/j.enconman.2014.01.020.

Isik, Z.M., Hüseyin, A., 2016. Analysis of ethanol RCCI application with safflower biodiesel blends in a high load diesel power generator. Fuel 184, 248–260. https://doi.org/10.1016/j.fuel.2016.07.017.

Ithnin, A.M., Ahmad, M.A., Bakar, M.A.A., Rajoo, S., Yahya, W.J., 2015. Combustion performance and emission analysis of diesel engine fuelled with water-in-diesel emulsion fuel made from low-grade diesel fuel. Energy Convers. Manag. 90, 375–382. https://doi.org/10.1016/j.enconman.2014.11.025.

Kakaee, A., Rahnama, P., Paykani, A., 2015. Influence of fuel composition on combustion and emissions characteristics of natural gas/diesel RCCI engine. J. Nat. Gas. Sci. Eng. 25, 58–65. https://doi.org/10.1016/j.jngse.2015.04.020.

Kavuri, C., Paz, J., Kokjohn, S.L., 2016. A comparison of Reactivity Controlled Compression Ignition (RCCI) and Gasoline Compression Ignition (GCI) strategies at high load, low speed conditions. Energy Convers. Manag. 127, 324–341. https://doi.org/10.1016/j.enconman.2016.09.026.

Lamb, J.J., 2020. Upgrading Biogas to Biomethane, in: Anaerobic Digestion. pp. 299–332. https://doi.org/10.48216/9788269203325ch9.

Li, J., Yang, W., Zhou, D., 2017. Review on the management of RCCI engines. Renew. Sustain. Energy Rev. 69, 65–79. https://doi.org/10.1016/j.rser.2016.11.159.

Li, J., Yang, W.M., Zhou, D.Z., 2016. Modeling study on the effect of piston bowl geometries in a gasoline/biodiesel fueled RCCI engine at high speed. Energy Convers. Manag. 112, 359–368. https://doi.org/10.1016/j.enconman.2016.01.041.

Li, P., Li, X., Wang, H., Guo, F., 2023. A comparative experimental study on emission characteristics and ammonia energy ratio of diesel generator operating in ammonia/diesel dual fuel mode by premixed and port injection. Process Saf. Environ. Prot. 176, 402–410. https://doi.org/10.1016/j.psep.2023.06.016.

Li, W., Liu, Z., Wang, Z., 2016. Experimental and theoretical analysis of the combustion process at low loads of a diesel natural gas dual-fuel engine. Energy 94, 728–741. https://doi.org/10.1016/j.energy.2015.11.052.

Li, Y., Alaimo, C.P., Kim, M., Kado, N.Y., Peppers, J., Xue, J., Wan, C., Green, P.G., Zhang, R., Jenkins, B.M., Vogel, C.F.A., Wuertz, S., Young, T.M., Kleeman, M.J., 2019. Composition and toxicity of biogas produced from different feedstocks in California. Environ. Sci. Technol. https://doi.org/10.1021/acs.est.9b03003.

Li, Y.Y., Li, H., Guo, H., Li, Y.Y., Yao, M., 2017. A numerical investigation on methane combustion and emissions from a natural gas-diesel dual fuel engine using CFD model. Appl. Energy 205, 153–162. https://doi.org/10.1016/j.apenergy.2017.07.071.

Lim, J.H., Reitz, R.D., 2014. High Load (21 Bar IMEP) Dual Fuel RCCI Combustion Using Dual Direct Injection. J. Eng. Gas. Turbines Power 136, 101514. https://doi.org/10.1115/1.4027361.

Mahmoodi, R., Yari, M., Ghafouri, J., Poorghasemi, K., 2020. Effect of reformed biogas as a low reactivity fuel on performance and emissions of a RCCI engine with reformed biogas/diesel dual-fuel combustion. Int. J. Hydrog. Energy. https://doi.org/10.1016/j.ijhydene.2020.09.183.

Meng, J., Xu, W., Meng, F., Wang, B., Zhao, P., Wang, Z., Ji, H., Yang, Y., 2023. Effects of waste cooking oil biodiesel addition on combustion, regulated and unregulated emission characteristics of common-rail diesel engine. Process Saf. Environ. Prot. 178, 1094–1106. https://doi.org/10.1016/j.psep.2023.08.065.

Merk, R., Heßelbach, K., Osipova, A., Popadić, D., Schmidt-Heck, W., Kim, G.J., Günther, S., Piñeres, A.G., Merfort, I., Humar, M., 2020. Particulate matter (Pm2.5) from biomass combustion induces an anti-oxidative response and cancer drug resistance in human bronchial epithelial beas-2b cells. Int. J. Environ. Res. Public Health 17, 1–22. https://doi.org/10.3390/ijerph17218193.

Milledge, J.J., Nielsen, B.V., Maneein, S., Harvey, P.J., 2019. A brief review of anaerobic digestion of algae for BioEnergy. Energies 12, 1–22. https://doi.org/10.3390/en12061166.

Montingelli, M.E., Tedesco, S., Olabi, A.G., 2015. Biogas production from algal biomass: A review. Renew. Sustain. Energy Rev. 43, 961–972. https://doi.org/10.1016/j.rser.2014.11.052.

Musa, M.A., Idrus, S., Harun, M.R., Marzuki, T.F.T.M., Wahab, A.M.A., 2020. A comparative study of biogas production from cattle slaughterhouse wastewater using conventional and modified upflow anaerobic sludge blanket (UASB) reactors. Int. J. Environ. Res. Public Health 17. https://doi.org/10.3390/ijerph17010283.

Nwokolo, N., Mukumba, P., Obileke, K., Enebe, M., 2020. Waste to energy: A focus on the impact of substrate type in biogas production. Processes 8, 1–21. https://doi.org/10.3390/pr8101224.

Paykani, A., Kakaee, A., Rahnama, P., Reitz, R.D., 2016. Progress and recent trends in reactivity-controlled compression ignition engines. Int. J. Engine Res. 17, 481–524. https://doi.org/10.1177/1468087415593013.

Polat, F., 2022. Experimental evaluation of the impacts of diesel-nanoparticles-waste tire pyrolysis oil ternary blends on the combustion, performance, and emission characteristics of a diesel engine. Process Saf. Environ. Prot. 160, 847–858. https://doi.org/10.1016/j.psep.2022.03.003.

Popadić, D., Heßelbach, K., Richter-Brockmann, S., Kim, G.J., Flemming, S., Schmidt-Heck, W., Häupl, T., Bonin, M., Dornhof, R., Achten, C., Günther, S., Humar, M., Merfort, I., 2018. Gene expression profiling of human bronchial epithelial cells exposed to fine particulate matter (PM2.5) from biomass combustion. Toxicol. Appl. Pharmacol. 347, 10–22. https://doi.org/10.1016/j.taap.2018.03.024.

Qian, Y., Zhang, Y., Wang, X., Lu, X., 2017. Particulate matter emission characteristics of a reactivity controlled compression ignition engine fueled with biogas/diesel dual fuel. J. Aerosol Sci. 113, 166–177. https://doi.org/10.1016/j.jaerosci.2017.08.003.

Rahnama, P., Paykani, A., Reitz, R.D., 2017. A numerical study of the effects of using hydrogen, reformer gas and nitrogen on combustion, emissions and load limits of a heavy duty natural gas/diesel RCCI engine. Appl. Energy 193, 182–198. https://doi.org/10.1016/j.apenergy.2017.02.023.

Rasi, S., 2009. Biogas Composition and upgrading to biomethane saija rasi biogas composition and upgrading to biomethane. Thesis Univ. Jyvask.

Said, M.A., Dalha, I.B., Abdul, Z.A., El-adawy, M., 2021. Influence of biogas mixing parameters on the combustion and emission characteristics of diesel RCCI engine. Alex. Eng. J. https://doi.org/10.1016/j.aej.2021.06.052.

Salahi, M.M., Esfahanian, V., Gharehghani, A., Mirsalim, M., 2017. Investigating the reactivity controlled compression ignition (RCCI) combustion strategy in a natural gas/diesel fueled engine with a pre-chamber. Energy Convers. Manag. 132, 40–53. https://doi.org/10.1016/j.enconman.2016.11.019.

Saxena, P., Jawale, S., Joshipura, M.H., 2013. A review on prediction of properties of biodiesel and blends of biodiesel. Procedia Eng. 51, 395–402. https://doi.org/10.1016/j.proeng.2013.01.055.

Shan, X., Qian, Y., Zhu, L., Lu, X., 2016. Effects of EGR rate and hydrogen/carbon monoxide ratio on combustion and emission characteristics of biogas/diesel dual fuel combustion engine. Fuel 181, 1050–1057. https://doi.org/10.1016/j.fuel.2016.04.132.

Sher, E., 1998. Environmental Aspects of Air Pollution. Handbook of Air Pollution From Internal Combustion Engines. Woodhead Publishing Limited,. https://doi.org/10.1016/b978-012639855-7/50041-7.

Soni, D.K., Gupta, R., 2016. Numerical investigation of emission reduction techniques applied on methanol blended diesel engine. Alex. Eng. J. 55, 1867–1879. https://doi.org/10.1016/j.aej.2016.02.019.

Tizvir, A., Shojaee fard, M.H., Molaeimanesh, G.R., Zahedi, A.R., Labbafi, S., 2023. Optimization of biodiesel production from microalgae and investigation of exhaust emissions and engine performance for biodiesel blended. Process Saf. Environ. Prot. 175, 319–340. https://doi.org/10.1016/j.psep.2023.05.056.

Ullah, I., Ha, M., Othman, D., Hashim, H., Matsuura, T., Ismail, A.F., Rezaei-dashtarzhandi, M., Azelee, I.W., 2017. Biogas as a renewable energy fuel – a review of biogas upgrading, utilisation and storage. Energy Convers. Manag. 150, 277–294. https://doi.org/10.1016/j.enconman.2017.08.035.

Wang, X., Qian, Y., Zhou, Q., Lu, X., 2016. Modulated diesel fuel injection strategy for efficient-clean utilization of low-grade biogas. Appl. Therm. Eng. 107, 844–852. https://doi.org/10.1016/j.applthermaleng.2016.07.057.

Wang, Y., Yao, M., Li, T., Zhang, W., Zheng, Z., 2016. A parametric study for enabling reactivity controlled compression ignition (RCCI) operation in diesel engines at various engine loads. Appl. Energy 175, 389–402. https://doi.org/10.1016/j.apenergy.2016.04.095.

Westbrook, C.K., 2000. Chemical kinetics of hydrocarbon ignition in practical combustion systems. Proc. Combust. Inst. 28, 1563–1577. https://doi.org/10.1016/s0082-0784(00)80554-8.

Wissink, M., Reitz, R.D., 2015. Direct dual fuel stratification, a path to combine the benefits of RCCI and PPC, 2015-01–0856 SAE Int. J. Engines 8. https://doi.org/10.4271/2015-01-0856.

Xu, Y., Huang, Y., Wu, B., Zhang, X., Zhang, S., 2015. Biogas upgrading technologies: Energetic analysis and environmental impact assessment. Chin. J. Chem. Eng. 23, 247–254. https://doi.org/10.1016/j.cjche.2014.09.048.

Zou, M., Dong, H., Zhu, Z., Zhan, Y., 2019. Optimization of ammonia stripping of piggery biogas slurry by response surface methodology. Int. J. Environ. Res. Public Health 16. https://doi.org/10.3390/ijerph16203819.